ACS EARTH AND SPACE CHEMISTRY

ACS EDITORS' CHOICE

http://pubs.acs.org/journal/aesccq

Article

Ambient Quantification and Size Distributions for Organic Aerosol in Aerosol Mass Spectrometers with the New Capture Vaporizer

Weiwei Hu, Pedro Campuzano-Jost, Douglas A. Day, Benjamin A. Nault, Taehyun Park, Taehyoung Lee, Aki Pajunoja, Annele Virtanen, Philip Croteau, Manjula R. Canagaratna, John T. Jayne, Douglas R. Worsnop, and Jose L. Jimenez*

Cite This: *ACS Earth Space Chem.* 2020, 4, 676−689

Read Online

ACCESS | Metrics & More | Article Recommendations | Supporting Information

ABSTRACT: Aerodyne aerosol mass spectrometers (AMSs) or aerosol chemical speciation monitors (ACSMs) are widely deployed to quantify organic aerosol (OA) mass concentration and size distribution in various field and laboratory studies across the world. A nonunity collection efficiency (CE, usually 0.45−1), resulting from particle bounce (PB) on a standard vaporizer (SV), depends on the chemical composition and phase of the aerosol. The estimation of CE contributes a significant fraction of the total quantification uncertainty for these instruments. To address this uncertainty, a capture vaporizer (CV) was recently designed to reduce or eliminate PB. Here, we evaluate the quantification of ambient submicron OA with the CV, including multiple biogenic- and anthropogenic-influenced field studies. Good agreement of OA between the SV and CV has been found (slopes = 0.84−1, $R > 0.9$), consistent with both CE ≈ 1 for ambient OA with the CV and with the chemical composition-dependent CE (CDCE) previously developed for ambient SV data. The effects of oxidation and thermal denuding of aerosols on quantification using both vaporizers are also examined. No effect of the oxidation state of OA on quantification of SV and CV AMSs is observed. Our results show that the SV CDCE, which works well for ambient aerosols, overestimates the CE of OA after thermal denuding because of nominally increasing inorganic acidity upon heating. Size distributions of three laboratory-generated OA species have similarly delayed detection and broadened ratios in the CV versus SV as for $(NH_4)_2SO_4$. The CV cannot measure size distributions at a lower vaporizer temperature (<500 °C for oleic acid and squalene and <350 °C for citric acid) because of too slow vaporization of OA. Finally, we summarize all the relevant pros and cons for using the CV versus SV in AMS and ACSM studies, which at present, point to the need to decide on the best vaporizer depending on the main objectives of a given instrument and study.

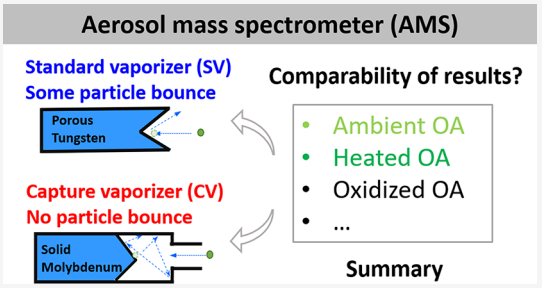

KEYWORDS: *OA quantification, size distribution, lens transimission, particle bounce, collection efficiency, oxidation flow reactor, OFR, thermodenuder, SOAS, KORUS-AQ*

1. INTRODUCTION

Organic aerosol (OA) accounts for 20−70% of the fine aerosol mass worldwide with an important impact on climate forcing and human health.[1−7] The quantification of total ambient OA, which is composed of thousands of individual species, has significant uncertainties for all methods.[8−13] This is due to the complex and dynamically varying physical and chemical properties of OA[7,13,14] and the general challenges in relation to quantitative collection of particles.[9,15] Aerosol mass spectrometers (AMSs) and/or aerosol chemical species monitors (ACSMs) are the only commercial instruments that can quantify total OA mass concentration with a time resolution of seconds to minutes.[16−23] Thus, these instruments are very commonly used in laboratory, for example, refs,[24,25] and field studies, for example, refs,[1,26] for OA quantification and chemical characterization. AMSs also can measure chemically resolved size distributions by measuring the particle flight time inside the AMS vacuum chamber.[20]

The commercialized standard vaporizer (SV) used in almost all AMSs and ACSMs is made of porous tungsten and shaped as a cylinder with an open inverted cone surface, where the particles impact and vaporize. Solid particles may not vaporize on the first collision and can bounce off the SV surface without evaporation, leading to incomplete particle detection. Thus, a correction factor based on the estimated collection efficiency (CE) is usually needed to account for particle bounce (PB) losses in the SV-AMS. CE varies with particle chemical composition and phase and can be measured or estimated in

Received: November 28, 2019
Revised: February 15, 2020
Accepted: February 17, 2020
Published: February 17, 2020

different ways, but inevitably introduces additional quantification uncertainty for aerosol concentration measurement.[27−30] Total uncertainties of ±38% (±35%) for ambient OA (inorganics) are estimated through uncertainty propagation, with a major contribution of the CE uncertainty.[8]

To reduce the uncertainties in SV-AMS quantification, a new capture vaporizer (CV) has been recently developed.[31] In the CV, nonrefractory particles go first through a narrow entrance into a cavity; then, the particles impact on a cone-like vaporizer surface (made of molybdenum) within the cavity, designed to maximize the fraction of particles captured. Solid particles can bounce around in the cavity until they are eventually vaporized. Schematics of the CV and SV are shown in Figure S1.

Recently, multiple field and laboratory studies have compared the performance of the SV and CV. Analysis of field studies showed CE ≈ 1 for the CV-AMS for ambient total and inorganic aerosols by comparing AMS measurements with other cosampled independent ion chromatography or volume measurements.[32,33] However, the CE of ambient OA in the CV has not yet been thoroughly investigated. CV data show increased decomposition/fragmentation of the sampled molecules for both inorganic[32,34,35] and organic species,[36,37] which is attributed to additional thermal decomposition and fragmentation.

In this study, we compare ambient OA mass concentration measured by collocated CV-AMS and SV-AMS (and also vs other indirect OA measurements, when available) in three diverse field studies. In addition, we investigated how OA processing by oxidation [using an oxidation flow reactor (OFR)] and evaporation [using a thermodenuder (TD)] can impact quantification of ambient OA and of other chemical components because particle morphology, phase, and volatility might change through these processing. The size distribution measurement of OA in the CV is also explored here in comparison to the SV. Finally, a summary of pros and cons on usage of the CV versus SV based on this study and previously published results is presented.

2. EXPERIMENTS

2.1. Field Studies. Three field studies are used in this analysis: (i) Southern Oxidant and Aerosol Study (SOAS); SOAS was conducted at a semipolluted ground site (Centreville, AL) surrounded by a forest in the southeast US during the summer of 2013.[38] OA in this study was typically dominated by the oxidation products of biogenic precursors (i.e., isoprene and monoterpenes)[39−42] with smaller contributions from urban primary OA (POA) and SOA[43,44] and biomass burning.[37] (ii) Billerica study, which was conducted in a suburban area of Boston (MA) in September 2012. The OA in this study was expected to be mainly impacted by urban emissions and mixed regional aerosols.[37] (3) The Korea-United States Air Quality mission (KORUS-AQ, May−June, 2016, an aircraft-based field campaign to examine the factors controlling air quality in and around the Seoul metropolitan area and Korean peninsula (research flights 05 and 11 used here). OA in this study is thought to be heavily impacted by anthropogenic sources, including some long-distance transport.[45,46]

2.2. Laboratory Studies. In laboratory studies, three standard organic compounds were tested for the size distribution experiments: squalene ($C_{30}H_{50}$; purity ≥99%; Sigma-Aldrich), oleic acid ($C_{18}H_{34}O_2$; purity ≥99%; Sigma-Aldrich), and citric acid ($C_6H_8O_7{\cdot}H_2O$; purity >99%; Fisher Scientific). Pure organic particles were generated through atomizing their solution with a Collison atomizer (model: 3076, TSI). Isopropanol (>99.5%, Sigma-Aldrich) was used as a solvent for squalene and oleic acid and water (Milli-Q) for citric acid. To remove the interference of solvents before AMS analysis, a silica gel diffusion dryer was used. This reduced the contribution of isopropanol to the organic particle signal below 5%, or it maintained relative humidity (RH) in the sampling line below 30%.

2.3. Instrumentation. *2.3.1. Aerosol mass spectrometer/aerosol chemical species monitor.* Two instruments using an SV and a CV were operated in parallel for all laboratory and field studies. High-resolution time-of-flight AMSs (HR-ToF-AMSs) were used for both the SV and CV in KORUS-AQ. A compact-ToF (C-ToF) AMS was used in SOAS for the CV versus an HR-ToF-AMS for the SV. Two quadrupole ACSMs equipped with the SV and CV were compared in the Billerica study. Detailed information on the instruments and operating conditions is given in Table S1.

For field studies, the ionization efficiency (IE) of AMS/ACSM was calibrated every few days with 400 nm monodisperse dried ammonium nitrate (NH_4NO_3) particles. The IE calibration methods of the brute-force single-particle mode[47] or event trigger, which are conducted by integrating multiple single-particle signals in the AMS, were used for the HR-ToF-AMS equipped with the SV. For the CV-AMS and both ACSMs, IE was calibrated using the alternative standard method by comparing the mass concentration determined from monodisperse condensation particle counter (CPC) particle counts versus the AMS signal.[18] IE calibrations in all studies were conducted simultaneously in the cosampling CV and SV instruments, using the same input flow of NH_4NO_3 particles. An exception is KORUS-AQ, where most calibrations were conducted separately, although a few times the instruments were calibrated together. Calibrations of particle size distributions were performed using polystyrene latex spheres (PSLs) and the output of a differential mobility analyzer (also calibrated with PSLs) in each study. ACSMs do not have particle sizing capacity. Detailed information on these calibrations can be found in previous papers.[32,35]

For all the field studies, chemical composition-dependent CE (CDCE, ∼0.5−0.7) was estimated for the SV[27] and a CE of 1 was used for the CV. A default OA-relative IE (RIE_{OA}, compared to nitrate) of 1.4 was used for both the CV and SV measurements.[48,50] Ammonium RIE was always calibrated by comparing its relative signal to that of nitrate when sampling pure NH_4NO_3. Sulfate RIE in each AMS/ACSM was calibrated by comparing relative signals of sulfate to ammonium when sampling pure $(NH_4)_2SO_4$ particles and assuming that the RIE of ammonium is the same as that for ammonium while sampling NH_4NO_3,[17,18] except SV-ACSM in Billerica that used a default value of 1.2. The oxygen-to-carbon (O/C) and hydrogen-to-carbon (H/C) ratios of OA for the SOAS SV-AMS were quantified with the improved ambient method reported by Canagaratna et al.[51]

2.3.2. OFR and TD. During the SOAS campaign, a potential aerosol mass OFR[52−54] was used to investigate OA formation/aging from ambient air[55−58] over a wide range of OH exposures (10^{10} to 10^{13} molec. cm^{-3} s). Also, a TD was used to investigate the volatility of OA.[59] The ambient, OFR, ambient, and TD lines were switched every 4 min for a total cycle of 20 min.

https://dx.doi.org/10.1021/acsearthspacechem.9b00310
ACS Earth Space Chem. 2020, 4, 676−689

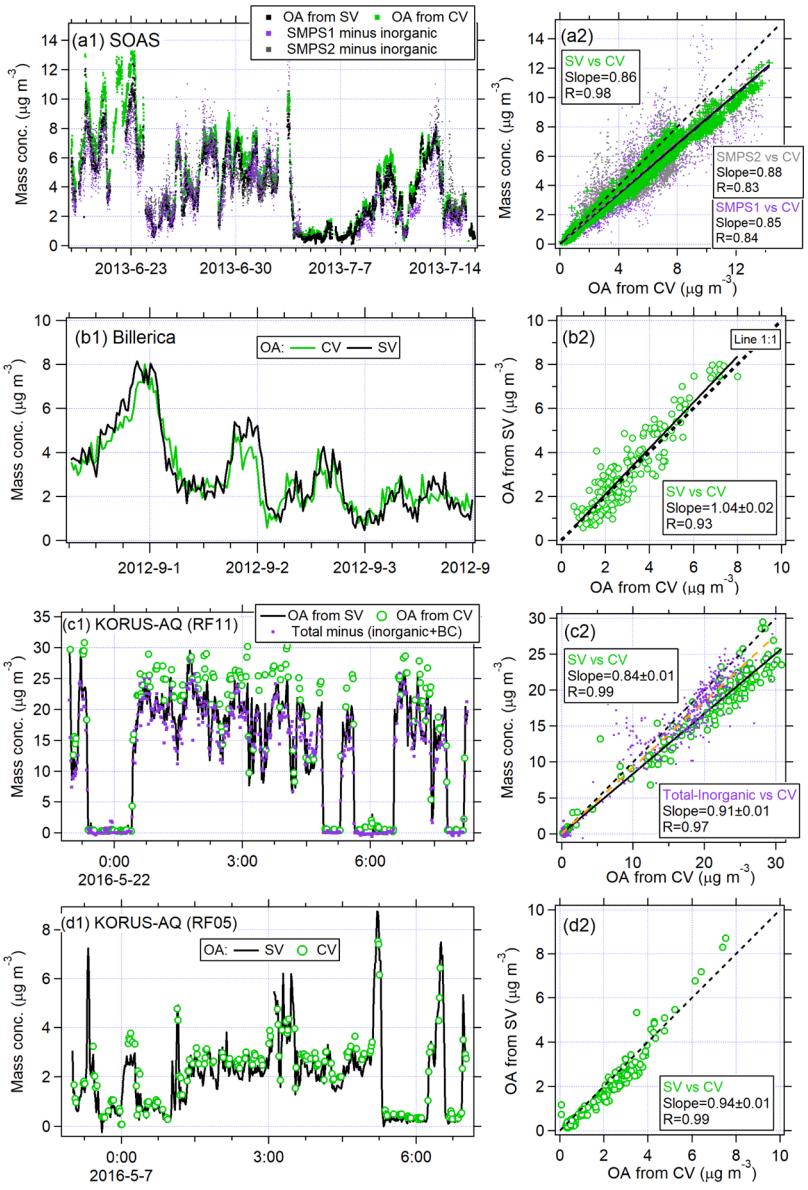

Figure 1. Time series and scatter plots of ambient OA using the CV and SV in the (a) SOAS, (b) Billerica, and (c,d) KORUS-AQ field studies. Results from two independent SMPS instruments are shown in SOAS. The time series of OA mass estimated as the difference between submicron mass measured using the SMPS in SOAS (or LAS in KORUS-AQ) and total inorganic mass from CV-AMS (and BC in KORUS, which was measured with a single-particle soot photometer, SP2) in each campaign are also shown to provide a separate estimate of OA concentrations. The BC is not subtracted from the total mass of the SMPS of SOAS because of its very low concentrations.[89] Orthogonal distance regression was applied in all the scatter plots here and in all latter figures. All the intercepts of the regression were forced to zero in all the scatter plots. For all the scatter plots, if the uncertainty of the regression slope is within 1%, the uncertainty is not shown [e.g., panel (a) in this figure], otherwise the corresponding uncertainty values are added as indicated in (panels b–d in this figure).

In the OFR, OH radicals were generated by 185 and 254 nm UV light that initiated O_2, H_2O, and O_3 photolysis in the "OFR185" mode of operation.[54,60] New SOA was formed from oxidation of ambient organic gases by OH radicals in the presence of ambient aerosols. Ambient and newly formed OA can also be oxidized through heterogeneous reaction with OH radicals. Very oxidized aerosols (O/C > 1) are typically observed for higher OH exposures (>1.1 × 10^{12} molec. cm^{-3} s).[57] In addition to OA, inorganic NH_4NO_3 and $(NH_4)_2SO_4$ were also formed by oxidation/partitioning of their gas-phase precursors NO_x, SO_2, and NH_3. More detailed information on OA chemistry in the OFR can be found in Hu et al. (2016) for SOAS and for similar studies in other forests.[55,56,61]

The temperature in the TD was increased linearly within the heating period (from 30 to 250 °C over 60 min) and then cooled down as quickly as possible with fans (60 min). The TD instrumentation and results are described in detail in previous publications.[59,62−64]

2.3.3. Other Instruments. Beside AMS/ACSM, we also used a scanning mobility particle sizer (SMPS; model: 3080, TSI, Shoreview, MN, US) in SOAS for submicron aerosol mass concentrations, which were estimated based on integrated volume concentration (calculated from the measured number size distribution) and aerosol densities estimated based on composition.[65,66] The range of particle mobility size (d_m) measured using an SMPS was ∼15 to ∼650−700 nm, which approximately corresponds to a vacuum aerodynamic

https://dx.doi.org/10.1021/acsearthspacechem.9b00310
ACS Earth Space Chem. 2020, 4, 676−689

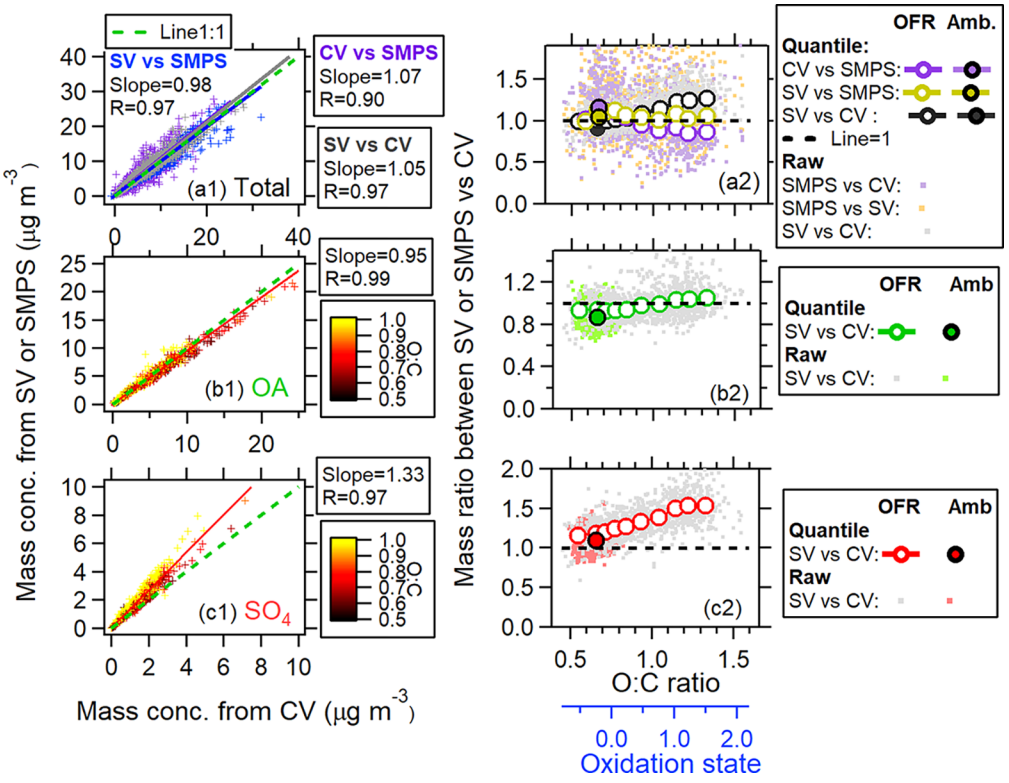

Figure 2. Scatter plots of ambient mass concentration of (a) total aerosol, (b) OA, and (c) SO_4 measured using the SV and CV in the output of the OH-OFR during SOAS. The mass ratios of these three species between the SV and CV as a function of the O/C ratio of OA are also shown. The axis of the carbon oxidation state (=2 × O/C−H/C) as the bottom axis is also added as a reference. In addition, mass ratios from ambient aerosols are also included. The error bar is the standard error. The time series comparisons of these species are shown in Figure S18.

size (d_{va}) range of ~20−1 μm.[67] Because the AMS cannot efficiently detect particles at d_{va} under 70 nm, we applied a lens transmission curve correction for particle d_{va} below 100 nm. Then lens transmission curve can be found in Figure S2. This is important for the OFR data set because strong new particle formation occurred in some cases, which can contribute ~10% of the total mass at high OH exposures (e.g., >5 × 10^{11} molec. cm^{-3} s) consistent with prior studies.[55] During KORUS-AQ, submicron aerosol mass concentration was estimated in the same way, but using number distributions from a laser aerosol spectrometer (LAS, model 3340, TSI Inc., US) instead of an SMPS.[46] The lower size cut of the LAS is around 170 nm, which can contribute up to ~8% of the difference of total aerosol between AMS and LAS systems in RF 11 reported here. For the higher size end, the AMS transmission curve was applied to calculate the appropriate volume concentration from the LAS.[46] An independent measure of the total aerosol mass or volume was not available for the Billerica study. The chemical composition-dependent density calculation for converting the SMPS or LAS volume concentration to mass concentrations is illustrated in detail in Section S1 of the Supporting Information (Figures S3 and S4). During SOAS, water-soluble organic carbon (WSOC) was measured with a PILS-total organic carbon analyzer.[68,69] The mass concentrations of water-soluble OA (WSOA) were estimated by multiplying the WSOC time series by that of OA/OC ratios from the SV-AMS.

3. RESULTS AND DISCUSSION

3.1. Quantification of Ambient OA. Ambient OA concentrations from the SV show strong correlation (R = 0.93−0.99) with those from the CV in all field studies, as shown in Figure 1. Regression slopes (0.84−1.04) are well within the quantification uncertainty of OA measured by SV-AMS (±38%, 2σ).[8] Note that the ±38% uncertainty cited here might be an overestimate for SV/CV comparisons because the RIE_{OA} uncertainty may partially cancel in these comparisons. In SOAS and KORUS-AQ, other independent measurements (e.g., WSOA in Figure S5 and OA calculated as the difference between the total aerosol mass measured with SMPS/LAS and total inorganic mass from the AMS in Figure 1) also show reasonable agreement and correlate well (slopes = 0.71−0.93; R > 0.83) with OA measured using the CV and SV. The good agreement among OA detected by CV-AMS, SV-AMS, and other independent measurements validates that CE ≈ 1 for ambient OA in the CV, consistent with a CE of ~1 for ambient total and inorganic aerosols reported previously.[35]

Note that all the AMS concentrations reported here are based on a default RIE_{OA} of 1.4. Good agreement for ambient OA comparisons of the SV versus CV and with non-AMS measurement in multiple field studies indicates that it is reasonable to use RIE_{OA} = 1.4 for the CV, consistent with the similarity of RIE_{OA} for laboratory tests of both vaporizers.[50] For specific OA compounds and in the absence of thermal decomposition, RIE_{OA} has been hypothesized to be dependent on the square root molecular weight ($\sqrt{MW}$);[70,71] however, empirical evidence for SV-AMS so far does not support that this effect is important for ambient OA, likely due to complex thermal decomposition/desorption effects or other complexities of the AMS detection process.[48] The three field studies shown here all have an average POA contribution of less than 20%.[37] Ambient OA that is strongly influenced by primary

https://dx.doi.org/10.1021/acsearthspacechem.9b00310
ACS Earth Space Chem. 2020, 4, 676−689

emissions (e.g., vehicle emission, biomass burning, and coal combustion) may have less thermal decomposition which might result in higher RIE_{OA},[10,48] for example, the RIE of cooking aerosols from chamber studies was found to be 1.5−3.1.[72] Evaluating CE × RIE with the SV or RIE more directly with the CV (CE = 1) for ambient OA in studies in which it is dominated by chemically reduced primary emissions is recommended for future studies.

3.2. OA Quantification as a Function of Its Oxidation Level. Oxidation can affect the quantification of OA in the AMS through changing the OA morphology/phase/hygroscopicity and its chemical structure, which can have large impacts on PB, thermal decomposition, and ionization in the AMS.[27,29,73] The quantification of ambient OA in the SV-AMS has been explored in multiple field studies;[8,10,27,65,74−76] however, only a few studies have focused on the effect of ambient OA quantification in the AMS as a function of its oxidation level, especially at high oxidation levels. Xu et al. (2018) showed a decreasing trend in RIE as a function of OA carbon oxidation state for reduced OA, followed by approximately constant values after mild oxidation.[49] Docherty et al.[29] reported a decreasing trend in CE (from 1 to ∼0.2) for chamber-generated SOA as the oxidation level of OA increased. Here, we take advantage of in situ measurement of OA as air was oxidized in the field-deployed OFR in the SOAS study[57] to provide the first comparison of ambient OA quantification in both the SV and CV as a function of the OA oxidation level (i.e., O/C ratio).

The ambient OA and newly formed SOA in the OFR were mainly constituted of isoprene- and monoterpene-derived SOA.[39,40,42,57] A wide range of O/C ratios in OA in the outflow of the OFR (0.6−1.5) was observed, depending on the OH exposure. Note that inorganic $(NH_4)_2SO_4$ and NH_4NO_3 were also formed in the OFR during this process because of the presence of ambient gas precursors of NH_3, SO_2, and NO_x,[55] albeit in smaller quantities relative to OA.

In general, good agreement of mass concentration is found between the SV and CV, and SMPS versus AMS for the total mass (slope = 0.93−1.05; $R > 0.90$, as shown in Figures 2 and S6), which is well within the combined quantification uncertainties of the SMPS and AMS (44%) in SOAS.[35] The ratios of both AMS versions against the SMPS are in agreement within measurement uncertainties as oxidation levels increase. However, slightly higher total SV/CV ratios are observed as OA O/C (0.5−1.5) increases in the OFR. This relative trend is mainly due to SO_4 and OA (Figure S7), for which the SV/CV ratios increase from 1.15 to 1.53 and 0.93 to 1.05, respectively (Figure 2).

To explore the potential reasons behind this relative difference between the SV and CV as a function of O/C, factors which control the quantification in the AMS are examined individually here. The equation to calculate the SV/CV mass ratios can be simply expressed as

$$\frac{\text{SV mass}}{\text{CV mass}} = \frac{\frac{\text{mass}_{(SV)}}{\text{IE}_{(SV)} \times \text{RIE}_{(SV)} \times \text{CE}_{(SV)}}}{\frac{\text{mass}_{(CV)}}{\text{IE}_{(CV)} \times \text{RIE}_{(CV)} \times \text{CE}_{(CV)}}} \quad (1)$$

where SV mass refers to the detected mass concentration and $\text{mass}_{(SV)}$ refers to the actual particle mass concentration sampled. IE is the ionization efficiency, which is a dimensionless quantity equaling the number of ions detected per molecule of the parent species. RIEs are defined as the relative IE of each species relative to nitrate because NH_4NO_3 is usually used for IE calibrations in the AMS.[17,18] CE is the collection efficiency as introduced above. Total CE < 1 in the AMS can be due to the limitations in lens transmission in the aerodynamic lens (E_l),[20,77] losses due to reduced focusing for nonspherical particles (E_s),[73] and PB loss at the vaporizer surfaces (E_b).[27,28] Thus, total CE can be expressed as[73]

$$\text{CE} = E_l \times E_s \times E_b \quad (2)$$

For ambient submicron aerosols, CE < 1 (∼0.5−1 for the SV) for submicron particles is mainly dominated by E_b and can be estimated from the chemical composition,[27] while the E_s loss is usually negligible.[73,78] The E_l can be calibrated with monodisperse particles with a comparison of CPC.[77] If the PM_1 AMS lens is working well and the particles sampled are in the size range of high lens transmission, E_l should be close to 1. For a well-functioning lens, the transmission curve should be similar to the values reported in Knote et al.[79] For the high end, complete transmission of particle sizes up to d_{va} = 550 nm and ∼50% of transmission for d_{va} = 1000 nm were found.

By combining eqs 1 and 2, we can obtain eq 3, as shown in the following

$$\frac{\text{SV mass}}{\text{CV mass}} = \frac{\frac{\text{mass}_{(SV)}}{\text{IE}_{(SV)} \times \text{RIE}_{(SV)} \times E_{b(SV)} \times E_{l(SV)} \times E_{s(SV)}}}{\frac{\text{mass}_{(CV)}}{\text{IE}_{(CV)} \times \text{RIE}_{(CV)} \times E_{b(CV)} \times E_{l(CV)} \times E_{s(CV)}}} \quad (3)$$

Overall changes of these six parameters can lead to a variation of the mass ratio between the SV versus CV. During the SOAS study, both the SV- and CV-AMSs were always sampled in parallel; thus, the $\text{mass}_{(SV)}$ and $\text{mass}_{(CV)}$ should be identical. The IE calibration based on NH_4NO_3 was conducted every few days (usually 3 days), which was very stable across the entire campaign when IE is normalized to the "air beam" (AB) signal (<3%) (AB, N_2^+ ion signal, is typically used as an internal reference).[35] The time cycle of OH exposure in the OFR was only around 2.5 h, which is a short enough period that the IE is not expected to significantly vary. Therefore, changes in IE should not influence the relative mass quantification of SO_4 and OA (or any other species) in the AMS as the OFR oxidation level is cycled through the full range of oxidant exposure.

As for the RIE of SO_4, the fragmentation pattern of SO_4 is stable across the entire range of OFR oxidation levels for both the SV and CV (Figure S8), suggesting that the vapors formed from SO_4 in the AMS do not change very much; hence, theoretically, the RIE of SO_4 should not change enough to affect the SV/CV ratios of SO_4. As for OA, an RIE change is possible because OA is becoming more functionalized upon oxidation, leading to more thermal decomposition in the AMS. Smaller molecular gas vapors from thermal decomposition could result in a smaller RIE of OA in the AMS,[48,70] although the extent to which this theoretical trend applies to real data is unclear, potentially due to additional effects in real instruments.[48,80,81] However, this RIE variation, if occurring, may vary similarly in both the SV and CV, potentially partially canceling out quantification bias because of effects of shifting RIE. The ambient OA in SOAS was already fairly oxidized (carbon oxidation state: −0.5 to 0.5). Xu et al. (2017) showed that when the oxidation state is in this range, the trend in the RIE of OA is small. Thus, although this study does not provide a direct measurement of the effect of RIE on OA

https://dx.doi.org/10.1021/acsearthspacechem.9b00310
ACS Earth Space Chem. 2020, 4, 676−689

quantification, the deviation caused by RIE change in OFR data set should be small.

The last three key parameters affecting quantification are E_b, E_s, and E_l, which will be discussed separately. For E_b, an $E_{b(CV)}$ of 1 is used in the CV, and the CDCE (~0.5−1) in the SV was empirically parametrized based on chemical composition and acidity of ambient aerosols. It is possible that there are changes of the particle phase at high OA oxidation levels that are not included in parameterization. If the aerosols become liquefied during aging,[82] the calculated CDCE (E_b) in the SV would lead to overestimation of the mass concentration in the SV. A higher SV/CV ratio could result if such process was occurring because a CE of 1 was expected for all the conditions in the CV.

To investigate the particle phase effect (E_b), SV/CV ratios of sulfate and OA as a function of PB fraction are shown in Figure S9. The PB fraction can be used to infer the particle phase.[83] During this campaign, PB fractions after OFR measurements were measured using an Aerosol Bounce Instruments (ABI) system developed by the University of Eastern Finland (see details in Section S2 in the Supporting Information).[82] Note that all the particles sampled using the AMS were dried under an RH of 40%, while sampling air for ABI is controlled around 50−60%. Thus, the particle phase in ABI measurement should be more liquid-like because of a higher water content[84] and also because of additional drying within the AMS. The SV/CV ratios exhibit a small increase in SO_4 (~10%) when PB values get lower. This increase is much lower than the ratio enhancement of SO_4 (33%) based on the SV/CV regression slope (Figure 2c). This suggests that an overestimation of CE in the SV because of changes in aerosol phase/morphology is not the main cause for increased SV/CV ratios after the OFR measurement.

We have shown that changes in RIE, IE, and E_b cannot fully explain the increased SV/CV ratios of SO_4. Based on the PB values, the phase/morphology of aerosol in the outflow of the OFR is supposed to be similar to or even more close to sphericity at higher O/C ratios.[85] Thus, extra losses due to the nonfocusing beam (E_s) should be negligible in both instruments. The only parameter left is E_l for both instruments. We speculate that different particle size cuts, that is, different lens transmissions, in two AMSs are the most likely reason to explain the variation of the mass ratio (SV/CV) as a function of O/C. As the peak of vacuum aerodynamic size (d_{va}) distribution of total aerosols measured with the SMPS increases as a function of O/C (Figures S3 and S10), a lower lens transmission efficiency in the CV than the SV for larger particles could lead to an SV/CV ratio increase. The impact on SO_4 is larger than that on OA because the size distribution of SO_4 is larger than that of OA (Figures S3 and S10), which is consistent with the higher ratio enhancement of SO_4 than of OA. The larger decrease of CV/SMPS ratios than the SV/SMPS ratios (Figure 2a2) also indicates that the CV might have a lower lens transmission efficiency at larger particle sizes than the SV. Unfortunately, the lens transmission calibration in the CV-AMS was not performed during the SOAS study, and from experience, it can change with time because of instrument transport and adjustment; therefore, we cannot prove our hypothesis with direct experimental measurement results.

Instead, we investigate this question based on simulating the variation of AMS/SMPS ratios by applying different AMS lens transmission curves to SMPS-integrated masses, as shown in Figure S2a.[32,79] The results in Figure S2b indeed show that the ratios between SMPS-integrated mass recalculated with different AMS lens transmission curves ($SMPS_{lens}$) and SMPS-integrated mass ($SMPS_{full\ size}$) are lower as a function of O/C ratios, which are similar to CV/SMPS ratios and indicate that the particle sizes are larger at higher O/C ratios. Also, the regression ratio ($SMPS_{lens}/SMPS_{full\ size}$ vs O/C) is lower when the AMS lens size cut is lower. Although the $SMPS_{lens}/SMPS_{full\ size}$ cannot fully capture the variation of CV/SMPS ratios, the similarity of variation trend of these two ratios as a function of O/C suggests that the different lens cuts are indeed one of the probable explanations for lower CV/SMPS or SV/CV ratios observed.

To simulate SO_4 particles, which have larger size distribution compared to OA (Figure S3), the original SMPS size distribution was shifted toward higher end with 30 nm (d_m); then, a similar analysis as discussed above was conducted. A faster decrease of the $SMPS_{lens}/SMPS_{full\ size}$ ratio has been found, as shown in Figure S2c,d. It is consistent with the larger increases of SV/CV ratios as a function of O/C observed for sulfate than OA. The uncertainty of SMPS measurement at a larger particle size (e.g., larger particle miscounted at different bins) and uncertainty of the AMS might also influence the variation of AMS/SMPS ratios.

The differences of lens transmission at the lower particle size cuts (<100 nm d_{va}) between the SV and CV could also possibly contribute to the higher SV/CV mass ratios. If the CV has a lower lens transmission efficiency at d_{va} of less than 100 nm than the SV, gradually increased SV/CV ratios as a function of O/C can be obtained because of enhanced masses at a lower size range (100 nm), contributed by stronger new particle formation at higher OH exposures in the OFR. However, the lower size cut should be a minor contributor for the mass differences because the SMPS showed that integrated mass with d_{va} less than 100 nm is around 10−15% of total mass for higher OH exposures, which is much lower than the mass differences of 33% in SO_4 comparison between the SV and CV.

In summary, the different lens size cuts (E_l) between the SV and CV-AMS is likely the main cause of the increased SV/CV ratios as a function of O/C in the OFR. Lens transmission curves leading to a mass discrepancy because of different size cuts (at either high or low ends) among different AMSs were observed frequently in multiple field studies.[32,46] Calibration of the lens transmission curve is recommended to be tested for every AMS instrument for better understanding the instrumentation performances and quantification.

3.3. Heating Influences on Quantification. The quantification of aerosols after evaporation in the TD is crucial in order to determine the accuracy of the aerosol volatilities. By heating aerosols in the TD, the chemical composition (and therefore acidity), phase/morphology, and volatility of aerosols could change, which can potentially lead to shifts of E_b and E_s in the AMS, and if not fully captured by the CDCE correction formulated for ambient nonheated aerosols,[27] errors in quantification could result. Here, we compare the SV and CV mass ratios for different aerosol components, together with AMS versus SMPS for total aerosol, as a function of TD temperature (T_{TD}, 35−230 °C) to evaluate if the CDCE correction is still applicable to the aerosol measurement after TD in the SV and test if the CE = 1 is still valid for TD measurements in CV-AMS.

During heating in the TD, NH_4 evaporated faster than the other species (i.e., SO_4 and NO_3), leading to a decrease of the

https://dx.doi.org/10.1021/acsearthspacechem.9b00310
ACS Earth Space Chem. 2020, 4, 676−689

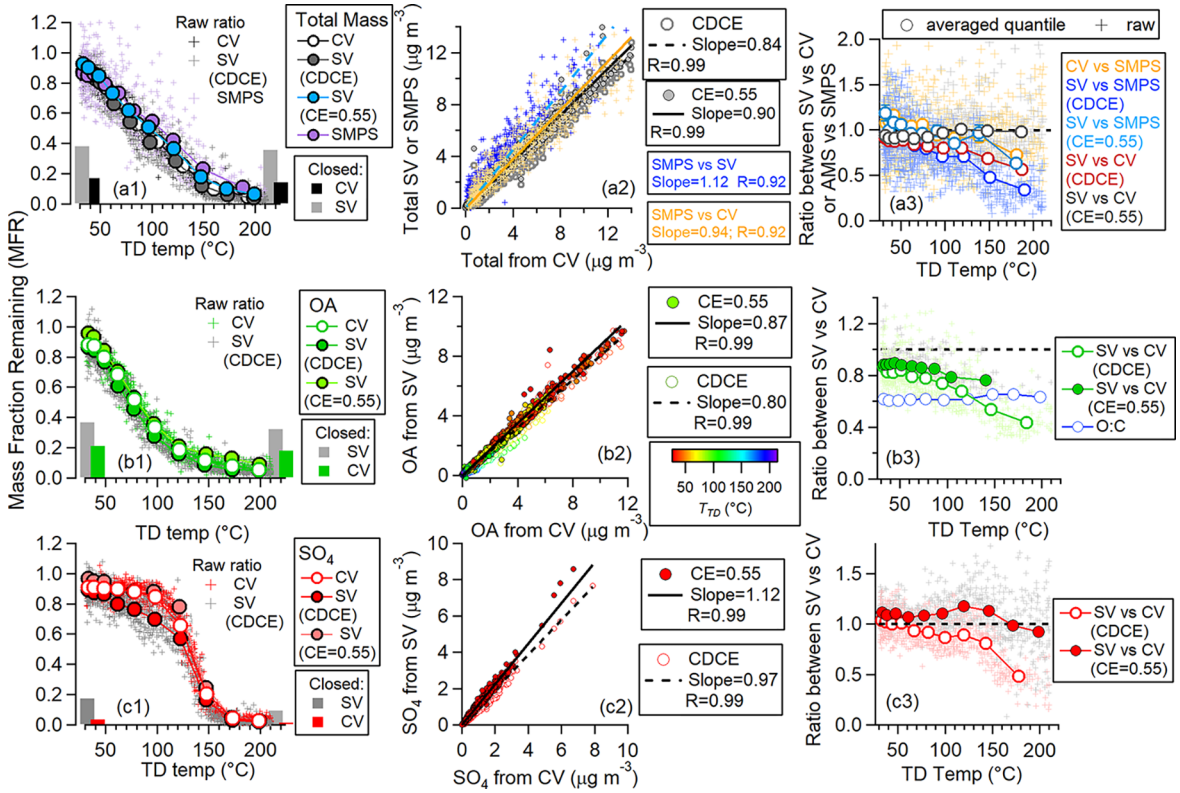

Figure 3. MFR as a function of TD temperature (T_{TD}), scatter plots, and mass ratios between the SV and CV after TD measurements for (a) total, (b) OA, and (c) SO_4 during the SOAS study. SV-AMS data corrected with CDCE and constant CE (=0.55) are both shown. The bars indicate the relative enhancement of AMS closed signal above the background after TD measurements at T_{TD} < 50 °C (left) and T_{TD} > 200 °C (right) vs the corresponding ambient signals. Lower bar values were found in the CV than the SV, suggesting a lower impact of sample aerosols on the instrument background in the former than the latter, consistent with prior results.[32] The error bar in this figure is the standard error.

measured cation/anion charge ratio (i.e., NH_4 aerosol acidity indicator, Figure S11), which is consistent with results reported in other ambient TD observations.[64] An increase in CDCE (dominated by E_b) from 0.5 to 1 as a function of T_{TD} was estimated because of enhanced aerosol acidity (parameterized by the SO_4/NH_4 ratios), as shown in Figure S11. For comparison, a constant CE of 0.55, obtained by averaging CDCE from ambient aerosols, was also applied to the SV-TD data set.

The thermograms, demonstrating the variations of mass fraction remaining (MFR) in total aerosols, OA, and SO_4, as a function of T_{TD}, are shown in Figure 3, together with scatter plots between the SV and CV. Generally, when the CDCE correction is applied, lower SV/CV regression ratios of the different main components are found in the TD compared to the ambient aerosols, for example, a regression ratio of 0.84 in the TD versus 0.90 in the ambient air for total aerosols, 0.80 versus 0.86 for OA, and 0.97 versus 1.07 for SO_4. In contrast, comparable or slightly higher SV/CV regression ratios (TD vs ambient air: 0.90 vs 0.90 for total aerosols; 0.87 vs 0.86 for OA; 1.12 vs 1.07 for SO_4) are obtained when constant CE is used in the analysis. The ratios between the SV and CV of total aerosols, OA, and SO_4 continuously decrease as a function of T_{TD} (from 35 to 230 °C) when the CDCE correction is applied. A slower decreasing trend for OA and quite stable ratios for total aerosol and SO_4 are observed when constant CE is applied in the SV. Total aerosol mass concentration from the SMPS is compared to the AMS total as an independent quantification reference in Figure 3a. The mass ratios between the CV and SMPS show a slight decrease as a function of T_{TD}, which is similar to the SV/SMPS with a constant CE correction; however, a faster decrease of SV/SMPS ratios with CDCE is observed when the CDCE is applied. This indicates that the CDCE parameterization of aerosol acidity appears not to be applicable to thermally denuded ambient particles.

To further investigate the T_{TD} effect on SV/CV (and also AMS vs SMPS), we examined the aerosol mass, RIE, IE, E_l, E_s, and E_b variations in both the SV and CV following eq 3. The same aerosol mass sampled, the stable IE/AB during the entire SOAS campaign (<3%), and the stable fragmentation patterns across different T_{TD} (Figure S12) suggest that mass, IE, and RIE are not the main reasons for the T_{TD}-dependent difference of SV/CV ratios. Very small aerosol size peak shrink due to heating is observed in the TD based on SMPS and AMS measurements (Figures S13 and S14). Similar to the OH OFR data set, we tested the impact of different lens cuts on the SMPS/AMS ratio by applying different lens transmission curves to SMPS data, as shown in Figure S15. Although the SMPS-integrated mass recalculated by different AMS lens transmission curves ($SMPS_{lens}$) has shown lower ratios than the SMPS-integrated mass at full size ($SMPS_{full\ size}$), the $SMPS_{lens}/SMPS_{full\ size}$ did not show a variation trend with TD temperature. It suggests that different lens transmission cuts can also not explain the decrease ratio of CV/SMPS and SV/SMPS (constant CE applied) as a function of T_{TD}.

The remaining explanations for the decreasing trend of CV/SMPS or SV/SMPS ratios with a constant CE applied as a function of T_{TD} changes in the aerosol volatility or phase/morphology upon heating, which is related to E_b and E_s. The

https://dx.doi.org/10.1021/acsearthspacechem.9b00310
ACS Earth Space Chem. 2020, 4, 676−689

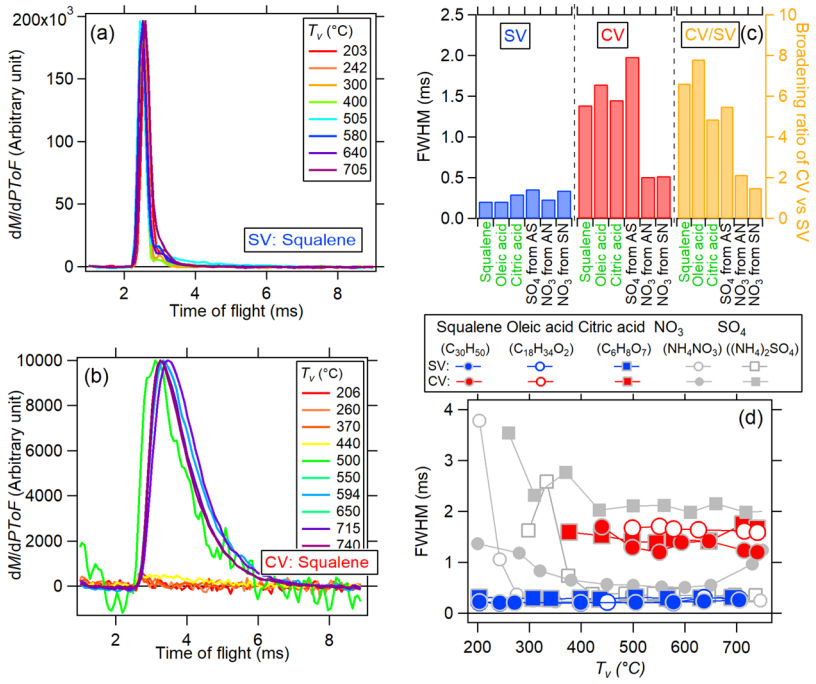

Figure 4. Size-resolved detection of the raw signal (using the PToF acquisition mode) of 300 nm squalene in the (a) SV and (b) CV as a function of T_v. (c) Left axis: calculated fwhm values for different pure OA species measured in the SV and CV at a vaporizer temperature (T_v) of 600 °C. For comparison, the fwhm ratio of the CV vs SV from pure 250 nm $(NH_4)_2SO_4$, 300 nm NH_4NO_3, and 300 nm $NaNO_3$ is also shown. Right axis: The fwhm ratios of the CV vs SV. (d) fwhm of squalene, oleic acid, citric acid, pure $(NH_4)_2SO_4$, and NH_4NO_3 as a function of T_v for the SV and CV. The results of inorganic species in Figure 5c,d are adapted from Hu et al.[32] The raw size distribution data for oleic acid and citric acid are shown in Figures S13 and S14.

volatility of OA species is continuously lower after semivolatile species leave particles as T_{TD} increases, which could result in additional PB losses (E_b) on the SV (but not the CV). For particle phase/morphology, it is hard to quantify the influence of how the phase/morphology changing upon heating will affect CE, although it could also play a role. Theoretically, the irregular-shaped particles (E_s) could lead to a wider particle beam; thus, they would result in additional particle loss because of some particles not hitting the vaporizer surface.[73] However, this effect on particle loss is supposed to be minor based on the experimental results that the 320 nm $(NH_4)_2SO_4$ beamwidth is well within 2 mm, which is less than the diameter of both the SV (3.81 mm) and CV (2.54 mm). The irregular-shaped particles could also lead to a higher bouncing fraction (E_b) when they hit on the vaporizer surfaces because of less thermal contacting areas.

In the SOAS study, the O/C ratios of OA stayed relatively constant as the TD temperature increases (Figure 3b3), which is quite different from increasing O/C ratios found in urban pollution studies.[64] On the other hand, it is similar to the biogenically originated SOA (e.g., SOA from α-pinene + O_3), which was found to have stable chemical composition in the TD[86,87] and evaporation experiments conducted in chambers.[88] For urban plumes, faster vaporization of POA (e.g., hydrocarbon-like OA, HOA) than SOA during the heating process was observed,[64] which is consistent with the increased abundance of low-volatile compounds as the heating proceeds. For biogenic SOA, it has been hypothesized that the stable O/C and chemical composition of aerosols upon heating are due to the following: (1) the low-volatile compounds were composed of oligomers, which have O/C values comparable to more volatile monomers;[88] (2) the heating-induced evaporation proceeds layer by layer because of diffusion limitation;[87] or (3) evaporation was controlled by the decomposition of oligomers, which contribute a high mass fraction of heated OA.[86,87]

In summary, based on the large decrease of SV/CV ratios as a function of T_{TD} when CDCE is applied, it seems that the parameterization of CDCE in ambient aerosols accounting for the acidity effect overestimates CE for thermally denuded aerosols. An averaged constant CE estimated based on cosampled nondenuded aerosol (or aerosols when T_{TD} is low, e.g., <50 °C) may be the best treatment if no additional information is available. That being said, a similar mass loss in the SV with either treatment is observed at higher T_{TD}. A more complex parameterization for CE in the TD accounting for changes in volatility, phase/morphology, and cation/anion charge ratio (NH_4 aerosol acidity) is recommended for future studies. The slightly lower CV/SMPS ratio as a function of T_{TD} indicates that there might be particle losses (<25%) in the CV at higher T_{TD} (>150 °C); however, for the majority of data, when T_{TD} is less than 150 °C, CE ≈ 1 in the CV appears to still be valid.

3.4. Particle Time-of-Flight Mode of Standard OA.

Broadened size distribution and delayed peak rise time for inorganic aerosols (e.g., NH_4NO_3 and $(NH_4)_2SO_4$) in the CV compared to the SV were reported in previous studies.[32,35] Similar broadening and delay effects have also been found in the size distribution of 300 nm standard OA species: squalene ($C_{30}H_{50}$, O/C = 0), oleic acid ($C_{18}H_{34}O_2$, O/C = 0.11), and citric acid ($C_6H_8O_7$, O/C = 1.17) in the CV (Figures 4 and S16 and S17), which is consistent with the longer residence time of particles and their gas vapors in the CV than the SV.

https://dx.doi.org/10.1021/acsearthspacechem.9b00310
ACS Earth Space Chem. 2020, 4, 676−689

Excellent Acceptable Less desirable

	SV	CV	Reference
CE for ambient particles	Middlebrook et al. (2012)	CE≈1	35
CE for pure inorganics in lab	Variable bounce fraction	< or ≈1 but better than SV	32; 34
Slowly evolving signals from bounced particles on colder ionizer surfaces	Significant	Nearly eliminated	32; 36
Ambient size distribution	Good resolution	Sufficient resolution	35
Lab & Chamber size distribution	Good resolution	Low resolution for monodisperse particles	32; This study
Single particle IE calibration	Most accurate	Not yet demonstrated	32
CPC-based IE calibration	Accurate	Accurate	35; 32
Extent of thermal decomposition	Significant	Greater than SV	35; 32; 36
Nitrate quantif. (organic vs. inorganic)	Useful even under low S/N	Less contrast and lower S/N	35
SO_4 UMR quantification under high OA	More OA interferences	Lower OA interferences	35
Nitrate → CO_2 artifact ("Pieber effect")	Important in some cases	Much lower for NH_4NO_3, similar for $NaNO_3$	32
Nitrate → Chloride artifact	Observable but small	Smaller than SV	35
CO^+/H_2O^+ artifact from OA	Not observed	Observed for reduced OA species	36
Elemental ratio for ambient aerosols	Good after applying reference calibration	Good after applying reference calibration	37
PMF factor separation	Reasonable	Reasonable, larger uncertainties for sub-OOA factors	37
OA tracer retained	Reasonable	Key tracers preserved.	36
Quantification upon heating	CDCE does not work. Constant CE is better	CE≈1	This study
OA quantification upon oxidation	Change in particle phase/morphology may introduce extra uncertainty	CE≈1	This study

Figure 5. Summary of the advantages and disadvantages of SV and CV usage in AMS/ACSM measurement based on this study and laboratory and field studies reported previously. Note that some effects should be further characterized in other instruments and studies.

The broadening ratio (BR) is defined as the ratio of size distribution width, calculated as full width at half-maximum (fwhm) of the distribution of particle time of flight (PToF, unit: ms), between the CV versus SV. The average BR is ~6.4 for the three OA species (range of ~5−7.8), which is similar to that for $(NH_4)_2SO_4$ (~5.5) and much higher than that for NH_4NO_3 (~2.1) and $NaNO_3$ (~1.8).[32] No consistent covariation of the broadened ratio between the CV and SV of different species versus their corresponding CE has been observed. Meanwhile, the delayed peak rise time of three OA species (~350 μs) is consistent with each other and also is similar to that of $(NH_4)_2SO_4$ (~450 ± 100 μs) and higher than that of NH_4NO_3 (~100 μs). The delayed peak rise time in the CV reflects the increased time spent by the vapors inside the CV compared to the SV. Both sets of data suggest that vaporized molecules adsorb and desorb one or several times for the CV, while that should be less frequent for SV. Slightly different peak rise times and peaking times were found for different ions in the CV (Figure S16), suggesting different impacts of surface adsorption and/or chemistry on the different species escaping the vaporizer (Figure S16). The similar broadened ratio and delayed peak rise time between OA and SO_4 suggest a consistent importance of surface processes for both sets of species.

The OA size distributions were also explored as a function of the vaporizer temperature (T_v) in both the SV and CV, as shown in Figure 4d. The fwhm in the SV does not show much variation across the entire T_v range (200−750 °C), with only slightly increased values at lower T_v (<300 °C), while the fwhm of OA in the CV shows consistently high and stable values compared to that in the SV when the size distribution is detectable. Unlike the SV, the size distribution of OA in the CV cannot be detected at lower T_v (<~420 °C for squalene and oleic acid; <~370 °C for citric acid), which might be due to the slow evaporation of these aerosols inside the CV under lower T_v.

4. PROS AND CONS FOR CV AND SV

Finally, we summarize the pros and cons on the usage of the CV versus SV based on this and previous studies shown in Figure 5. In summary, the CV and SV have different advantages and disadvantages for aerosol detection with the AMS. The CV generally improves aerosol quantification,[32,36] especially with complex effects on ambient aerosol (e.g., oxidation/heating), as shown in this study. For $PM_{2.5}$ measurement, the CV was necessary to quantify supermicron particles, which are observed to have higher and variable bounce in the SV, and thus are more difficult to quantify with the SV-AMS.[34] However, for chemically reduced aerosols, artifact ions (especially CO^+) formed through the chemical reaction between sampled OA with CV surfaces need to be excluded in aerosol quantifications.[36] The CV shows smaller CO_2^+ and chloride artifacts (when inorganic aerosol is sampled) than the SV.[32,35] Compared to the SV, the chemical information content of aerosols in the CV-AMS data is degraded because of greater thermal decomposition;[32,34−36] however, it is still sufficient for positive matrix factorization (PMF) and elemental ratio analysis.[37] The most commonly used tracer ion in the SV can still be used in the CV, albeit with reduced signal-to-noise ratio in some cases. The size distributions of different aerosol species are broadened in the CV, which is important for laboratory-generated monodisperse

https://dx.doi.org/10.1021/acsearthspacechem.9b00310
ACS Earth Space Chem. 2020, 4, 676−689

aerosols,[32] whereas it is of limited importance for ambient aerosols because ambient distributions are typically quite broad.[35] After proper calibration, particle sizing of the CV-AMS is still useful for ambient measurements,[35] for example, for size-dependent density calculation. More examination of size distribution comparisons for ambient aerosols is recommended. Overall, the comparison results between the SV and CV suggest that the AMS users should determine their own best vaporizer based on their main purpose of experiments.

5. CONCLUSIONS

The quantification of OA in the CV and SV has been examined in multiple ambient field studies. The OA mass concentrations from the CV (CE = 1) show good agreement (regression slope = 0.83−1, R > 0.83) with OA from the SV (CDCE, 0.5−0.7 applied) and total mass measured with the SMPS minus inorganic species from the AMS, suggesting a complete capture of the OA mass concentrations with the CV-AMS. In this study, we only examined the quantification of ambient aerosols in the CV under biogenic- and anthropogenic-influenced areas with SOA dominating the OA (>80%). The CE and RIE quantification of different types of primary aerosols from specific sources, such as biomass burning, coal combustion, and cooking are recommended for future studies. SOA from specific chamber studies are also recommended for the future studies.

We also explored the performance of OA quantification under the impact of OA oxidation and heating during the SOAS study using a field-deployed OFR and TD, respectively. Higher mass ratios of SV/CV as a function of O/C ratios were observed to varying degrees for different components. The differences in the lens cut (E_l) between the SV-AMS and CV-AMS (or AMS vs SMPS) are likely the main reason for the trends in ratios of the SV versus CV mass concentration because of particle growth beyond the AMS size cut during aging. Lens transmission differences at smaller sizes (d_{va} < 100 nm) is a possible cause; however, it is supposed to have a smaller effect because of smaller mass contribution within this range.

In the TD (35−230 °C), a decreasing trend of the SV/CV ratios (and AMS/SMPS) with temperature is observed. The larger reduced mass in the SV-AMS is mainly caused by the extra PBs (E_b) in the SV because of lower aerosol volatility and/or irregular particle phase/morphology after heating. Much lower SV/CV mass ratios are found when the CDCE correction method (derived from ambient, nonheated data; Middlebrook et al. 2012) is applied using the denuded aerosol chemical composition than simply applying a constant CE used for the SV, suggesting that the standard CDCE correction is not suitable for the quantification of heated aerosols in the SV.[29]

The measured size distributions of pure standard OA compounds (i.e., squalene, oleic acid, and citric acid) in the CV are much more broadened than those in the SV, which is consistent with that found for inorganic species. The average broadened ratio (=fwhm ratio between CV and SV) of OA is 6.4, which is similar to that of $(NH_4)_2SO_4$ (∼5.5) and much higher than that of NH_4NO_3 and $NaNO_3$ (∼2). OA size distribution in the CV cannot be detected at a lower vaporizer temperature (<350 °C for citric acid and <500 °C for oleic acid and squalene) because of the slow vaporization of OA. Finally, we summarized the pros and cons for using the SV and CV in the AMS. We found CV-improved aerosol quantification and generally show similar chemical information as the SV for ambient aerosols.

■ ASSOCIATED CONTENT

Supporting Information

The Supporting Information is available free of charge at https://pubs.acs.org/doi/10.1021/acsearthspacechem.9b00310.

AMS types, vaporizer temperature, and time resolution of AMSs; schematic of the standard vaporizer and capture vaporizer; mass-based size distribution; aerodynamic size comparison ; equation-estimated OA density versus measured bulk OA density; time series and scatter plots; difference between the SV and CV; fragmentation pattern of sulfate as a function of O/C ratios; time series of particle bounce; mobility size distribution of total aerosol; chemical composition-based CE and NH_4 balance; fragmentation pattern of sulfate; comparison of aerodynamic size distribution; size-resolved detection of raw data for major ions; and time series of total mass concentration (PDF)

■ AUTHOR INFORMATION

Corresponding Author

Jose L. Jimenez − *Cooperative Institute for Research in the Environmental Sciences (CIRES) and Department of Chemistry & Biochemistry, University of Colorado at Boulder, Boulder, Colorado 80309, United States;* orcid.org/0000-0001-6203-1847; Email: jose.jimenez@colorado.edu

Authors

Weiwei Hu − *State Key Laboratory of Organic Geochemistry, Guangzhou Institute of Geochemistry, Chinese Academy of Sciences, Guangzhou 510640, China; Cooperative Institute for Research in the Environmental Sciences (CIRES) and Department of Chemistry & Biochemistry, University of Colorado at Boulder, Boulder, Colorado 80309, United States;* orcid.org/0000-0002-3485-6304

Pedro Campuzano-Jost − *Cooperative Institute for Research in the Environmental Sciences (CIRES) and Department of Chemistry & Biochemistry, University of Colorado at Boulder, Boulder, Colorado 80309, United States;* orcid.org/0000-0003-3930-010X

Douglas A. Day − *Cooperative Institute for Research in the Environmental Sciences (CIRES) and Department of Chemistry & Biochemistry, University of Colorado at Boulder, Boulder, Colorado 80309, United States;* orcid.org/0000-0003-3213-4233

Benjamin A. Nault − *Cooperative Institute for Research in the Environmental Sciences (CIRES) and Department of Chemistry & Biochemistry, University of Colorado at Boulder, Boulder, Colorado 80309, United States;* orcid.org/0000-0001-9464-4787

Taehyun Park − *Department of Environmental Science, Hankuk University of Foreign Studies, Yongin 17035, South Korea;* orcid.org/0000-0002-1030-7618

Taehyoung Lee − *Department of Environmental Science, Hankuk University of Foreign Studies, Yongin 17035, South Korea*

Aki Pajunoja − *Department of Applied Physics, University of Eastern Finland, Kuopio 70210, Finland*

https://dx.doi.org/10.1021/acsearthspacechem.9b00310
ACS Earth Space Chem. 2020, 4, 676−689

Annele Virtanen − *Department of Applied Physics, University of Eastern Finland, Kuopio 70210, Finland*
Philip Croteau − *Aerodyne Research, Inc., Billerica, Massachusetts 01821, United States*
Manjula R. Canagaratna − *Aerodyne Research, Inc., Billerica, Massachusetts 01821, United States*
John T. Jayne − *Aerodyne Research, Inc., Billerica, Massachusetts 01821, United States*
Douglas R. Worsnop − *Aerodyne Research, Inc., Billerica, Massachusetts 01821, United States*

Complete contact information is available at: https://pubs.acs.org/10.1021/acsearthspacechem.9b00310

Notes

The authors declare no competing financial interest.

■ ACKNOWLEDGMENTS

This research was partially supported by NASA 80NSSC19K0124, NSF AGS-1822664, and a CIRES IRP grant. Development of the CV device was supported by the U.S. Dept. of Energy SBIR program DE-SC0001673. We sincerely thank the DC-8 crew and DC-8 science team for their help and support during the KORUS-AQ study and Hongyu Guo and Rodney Weber from Georgia Tech for SOAS WSOC data support, as well as Bruce Anderson, Andreas J. Beyersdorf, Chelsea A. Corr and Kenneth L. Thornhill from NASA Langley Research Center for KORUS-AQ LAS data support.

■ REFERENCES

(1) Jimenez, J. L.; Canagaratna, M. R.; Donahue, N. M.; Prevot, A. S. H.; Zhang, Q.; Kroll, J. H.; DeCarlo, P. F.; Allan, J. D.; Coe, H.; Ng, N. L.; Aiken, A. C.; Docherty, K. S.; Ulbrich, I. M.; Grieshop, A. P.; Robinson, A. L.; Duplissy, J.; Smith, J. D.; Wilson, K. R.; Lanz, V. A.; Hueglin, C.; Sun, Y. L.; Tian, J.; Laaksonen, A.; Raatikainen, T.; Rautiainen, J.; Vaattovaara, P.; Ehn, M.; Kulmala, M.; Tomlinson, J. M.; Collins, D. R.; Cubison, M. J.; Dunlea, J.; Huffman, J. A.; Onasch, T. B.; Alfarra, M. R.; Williams, P. I.; Bower, K.; Kondo, Y.; Schneider, J.; Drewnick, F.; Borrmann, S.; Weimer, S.; Demerjian, K.; Salcedo, D.; Cottrell, L.; Griffin, R.; Takami, A.; Miyoshi, T.; Hatakeyama, S.; Shimono, A.; Sun, J. Y.; Zhang, Y. M.; Dzepina, K.; Kimmel, J. R.; Sueper, D.; Jayne, J. T.; Herndon, S. C.; Trimborn, A. M.; Williams, L. R.; Wood, E. C.; Middlebrook, A. M.; Kolb, C. E.; Baltensperger, U.; Worsnop, D. R. Evolution of Organic Aerosols in the Atmosphere. *Science* **2009**, *326*, 1525−1529 and references therein.
(2) Murphy, D. M.; Cziczo, D. J.; Hudson, P. K.; Thomson, D. S. Carbonaceous material in aerosol particles in the lower stratosphere and tropopause region. *J. Geophys. Res.: Atmos.* **2007**, *112*, D04203.
(3) Kanakidou, M.; Seinfeld, J. H.; Pandis, S. N.; Barnes, I.; Dentener, F. J.; Facchini, M. C.; Van Dingenen, R.; Ervens, B.; Nenes, A.; Nielsen, C. J.; Swietlicki, E.; Putaud, J. P.; Balkanski, Y.; Fuzzi, S.; Horth, J.; Moortgat, G. K.; Winterhalter, R.; Myhre, C. E. L.; Tsigaridis, K.; Vignati, E.; Stephanou, E. G.; Wilson, J. Organic aerosol and global climate modelling: a review. *Atmos. Chem. Phys.* **2005**, *5*, 1053−1123.
(4) Pöschl, U. Atmospheric aerosols: Composition, transformation, climate and health effects. *Angew. Chem., Int. Ed.* **2005**, *44*, 7520−7540.
(5) IPCC. *Intergovernmental Panel on Climate Change (IPCC): Climate Change: The Scientific Basis*; Cambridge University Press: U.K., 2017.
(6) Mauderly, J. L.; Chow, J. C. Health Effects of Organic Aerosols. *Inhalation Toxicol.* **2008**, *20*, 257−288.
(7) Geiger, F.; Pope, F.; MacKenzie, R.; Brune, W.; Monks, P. S.; Bloss, W.; Fuller, G.; Moussiopoulos, N.; Hort, M.; Tomlin, A.; Presto, A.; van Pinxteren, D.; Vlachou, A.; Heard, D.; Hewitt, C. N.; Baltensperger, U.; Lewis, A.; Querol, X.; Kim, S.; Hamilton, J.; Sommariva, R.; McFiggans, G.; Harrison, R.; Jimenez, J. L.; Cross, E.; Wenger, J.; Pandis, S.; Kiendler-Scharr, A.; Donahue, N. M.; Whalley, L.; McDonald, B.; Pieber, S.; Prevot, A.; Alam, M. S.; Krishna Kumar, N.; Wahner, A.; Skouloudis, A.; Kalberer, M.; Wallington, T.; Dunmore, R. Chemical complexity of the urban atmosphere and its consequences: general discussion. *Faraday Discuss.* **2016**, *189*, 137.
(8) Bahreini, R.; Ervens, B.; Middlebrook, A. M.; Warneke, C.; de Gouw, J. A.; DeCarlo, P. F.; Jimenez, J. L.; Brock, C. A.; Neuman, J. A.; Ryerson, T. B.; Stark, H.; Atlas, E.; Brioude, J.; Fried, A.; Holloway, J. S.; Peischl, J.; Richter, D.; Walega, J.; Weibring, P.; Wollny, A. G.; Fehsenfeld, F. C. Organic aerosol formation in urban and industrial plumes near Houston and Dallas, Texas. *J. Geophys. Res.: Atmos.* **2009**, *114*, D00F16.
(9) Turpin, B. J.; Saxena, P.; Andrews, E. Measuring and simulating particulate organics in the atmosphere: problems and prospects. *Atmos. Environ.* **2000**, *34*, 2983−3013.
(10) Docherty, K. S.; Aiken, A. C.; Huffman, J. A.; Ulbrich, I. M.; DeCarlo, P. F.; Sueper, D.; Worsnop, D. R.; Snyder, D. C.; Peltier, R. E.; Weber, R. J.; Grover, B. D.; Eatough, D. J.; Williams, B. J.; Goldstein, A. H.; Ziemann, P. J.; Jimenez, J. L. The 2005 Study of Organic Aerosols at Riverside (SOAR-1): instrumental intercomparisons and fine particle composition. *Atmos. Chem. Phys.* **2011**, *11*, 12387−12420.
(11) McMurry, P. A review of atmospheric aerosol measurements. *Atmos. Environ.* **2000**, *34*, 1959−1999.
(12) Chow, J. C.; Watson, J. G.; Chen, L.-W. A.; Rice, J.; Frank, N. H. Quantification of $PM_{2.5}$ organic carbon sampling artifacts in US networks. *Atmos. Chem. Phys.* **2010**, *10*, 5223−5239.
(13) Hallquist, M.; Wenger, J. C.; Baltensperger, U.; Rudich, Y.; Simpson, D.; Claeys, M.; Dommen, J.; Donahue, N. M.; George, C.; Goldstein, A. H.; Hamilton, J. F.; Herrmann, H.; Hoffmann, T.; Iinuma, Y.; Jang, M.; Jenkin, M. E.; Jimenez, J. L.; Kiendler-Scharr, A.; Maenhaut, W.; McFiggans, G.; Mentel, T. F.; Monod, A.; Prévôt, A. S. H.; Seinfeld, J. H.; Surratt, J. D.; Szmigielski, R.; Wildt, J. The formation, properties and impact of secondary organic aerosol: current and emerging issues. *Atmos. Chem. Phys.* **2009**, *9*, 5155−5236.
(14) Ziemann, P. J.; Atkinson, R. Kinetics, products, and mechanisms of secondary organic aerosol formation. *Chem. Soc. Rev.* **2012**, *41*, 6582−6605.
(15) Quinn, P. K.; Bates, T. S.; Coffman, D.; Onasch, T. B.; Worsnop, D.; Baynard, T.; de Gouw, J. A.; Goldan, P. D.; Kuster, W. C.; Williams, E.; Roberts, J. M.; Lerner, B.; Stohl, A.; Pettersson, A.; Lovejoy, E. R. Impacts of sources and aging on submicrometer aerosol properties in the marine boundary layer across the Gulf of Maine. *J. Geophys. Res.: Atmos.* **2006**, *111*, D23S36.
(16) Allan, J. D.; Alfarra, M. R.; Bower, K. N.; Williams, P. I.; Gallagher, M. W.; Jimenez, J. L.; McDonald, A. G.; Nemitz, E.; Canagaratna, M. R.; Jayne, J. T.; Coe, H.; Worsnop, D. R. Quantitative sampling using an Aerodyne aerosol mass spectrometer - 2. Measurements of fine particulate chemical composition in two U.K. cities. *J. Geophys. Res.: Atmos.* **2003**, *108*, 4091.
(17) Jimenez, J. L.; Jayne, J. T.; Shi, Q.; Kolb, C. E.; Worsnop, D. R.; Yourshaw, I.; Seinfeld, J. H.; Flagan, R. C.; Zhang, X. F.; Smith, K. A.; Morris, J. W.; Davidovits, P. Ambient aerosol sampling using the Aerodyne Aerosol Mass Spectrometer. *J. Geophys. Res.: Atmos.* **2003**, *108*, 8425.
(18) Canagaratna, M. R.; Jayne, J. T.; Jimenez, J. L.; Allan, J. D.; Alfarra, M. R.; Zhang, Q.; Onasch, T. B.; Drewnick, F.; Coe, H.; Middlebrook, A.; Delia, A.; Williams, L. R.; Trimborn, A. M.; Northway, M. J.; DeCarlo, P. F.; Kolb, C. E.; Davidovits, P.; Worsnop, D. R. Chemical and microphysical characterization of ambient aerosols with the aerodyne aerosol mass spectrometer. *Mass Spectrom. Rev.* **2007**, *26*, 185−222.
(19) Drewnick, F.; Schwab, J. J.; Hogrefe, O.; Peters, S.; Husain, L.; Diamond, D.; Weber, R.; Demerjian, K. L. Intercomparison and evaluation of four semi-continuous PM2.5 sulfate instruments. *Atmos. Environ.* **2003**, *37*, 3335−3350.
(20) Jayne, J. T.; Leard, D. C.; Zhang, X.; Davidovits, P.; Smith, K. A.; Kolb, C. E.; Worsnop, D. R. Development of an aerosol mass

spectrometer for size and composition analysis of submicron particles. *Aerosol Sci. Technol.* **2000**, *33*, 49−70.
(21) Kimmel, J. R.; Farmer, D. K.; Cubison, M. J.; Sueper, D.; Tanner, C.; Nemitz, E.; Worsnop, D. R.; Gonin, M.; Jimenez, J. L. Real-time aerosol mass spectrometry with millisecond resolution. *Int. J. Mass Spectrom.* **2011**, *303*, 15−26.
(22) Ng, N. L.; Herndon, S. C.; Trimborn, A.; Canagaratna, M. R.; Croteau, P. L.; Onasch, T. B.; Sueper, D.; Worsnop, D. R.; Zhang, Q.; Sun, Y. L.; Jayne, J. T. An Aerosol Chemical Speciation Monitor (ACSM) for Routine Monitoring of the Composition and Mass Concentrations of Ambient Aerosol. *Aerosol Sci. Technol.* **2011**, *45*, 780−794.
(23) Fröhlich, R.; Cubison, M. J.; Slowik, J. G.; Bukowiecki, N.; Prévôt, A. S. H.; Baltensperger, U.; Schneider, J.; Kimmel, J. R.; Gonin, M.; Rohner, U.; Worsnop, D. R.; Jayne, J. T. The ToF-ACSM: a portable aerosol chemical speciation monitor with TOFMS detection. *Atmos. Meas. Tech.* **2013**, *6*, 3225−3241.
(24) Grieshop, A. P.; Logue, J. M.; Donahue, N. M.; Robinson, A. L. Laboratory investigation of photochemical oxidation of organic aerosol from wood fires 1: measurement and simulation of organic aerosol evolution. *Atmos. Chem. Phys.* **2009**, *9*, 1263−1277 and references therein.
(25) Daumit, K. E.; Carrasquillo, A. J.; Hunter, J. F.; Kroll, J. H. Laboratory studies of the aqueous-phase oxidation of polyols: submicron particles vs. bulk aqueous solution. *Atmos. Chem. Phys.* **2014**, *14*, 10773−10784 and references therein.
(26) Zhang, Q.; Jimenez, J. L.; Canagaratna, M. R.; Allan, J. D.; Coe, H.; Ulbrich, I.; Alfarra, M. R.; Takami, A.; Middlebrook, A. M.; Sun, Y. L.; Dzepina, K.; Dunlea, E.; Docherty, K.; DeCarlo, P. F.; Salcedo, D.; Onasch, T.; Jayne, J. T.; Miyoshi, T.; Shimono, A.; Hatakeyama, S.; Takegawa, N.; Kondo, Y.; Schneider, J.; Drewnick, F.; Borrmann, S.; Weimer, S.; Demerjian, K.; Williams, P.; Bower, K.; Bahreini, R.; Cottrell, L.; Griffin, R. J.; Rautiainen, J.; Sun, J. Y.; Zhang, Y. M.; Worsnop, D. R. Ubiquity and dominance of oxygenated species in organic aerosols in anthropogenically-influenced Northern Hemisphere midlatitudes. *Geophys. Res. Lett.* **2007**, *34*, L13801 and references therein.
(27) Middlebrook, A. M.; Bahreini, R.; Jimenez, J. L.; Canagaratna, M. R. Evaluation of Composition-Dependent Collection Efficiencies for the Aerodyne Aerosol Mass Spectrometer using Field Data. *Aerosol Sci. Technol.* **2012**, *46*, 258−271.
(28) Matthew, B. M.; Middlebrook, A. M.; Onasch, T. B. Collection efficiencies in an Aerodyne Aerosol Mass Spectrometer as a function of particle phase for laboratory generated aerosols. *Aerosol Sci. Technol.* **2008**, *42*, 884−898.
(29) Docherty, K. S.; Jaoui, M.; Corse, E.; Jimenez, J. L.; Offenberg, J. H.; Lewandowski, M.; Kleindienst, T. E. Collection Efficiency of the Aerosol Mass Spectrometer for Chamber-Generated Secondary Organic Aerosols. *Aerosol Sci. Technol.* **2013**, *47*, 294−309.
(30) Robinson, E. S.; Onasch, T. B.; Worsnop, D.; Donahue, N. M. Collection efficiency of α-pinene secondary organic aerosol particles explored via light-scattering single-particle aerosol mass spectrometry. *Atmos. Meas. Tech.* **2017**, *10*, 1139−1154.
(31) Jayne, J. T.; Worsnop, D. R. Particle Capture Device. U.S. Patent 20,150,040,689 A1; Aerodyne Research, Inc., 2016.
(32) Hu, W.; Campuzano-Jost, P.; Day, D. A.; Croteau, P.; Canagaratna, M. R.; Jayne, J. T.; Worsnop, D. R.; Jimenez, J. L. Evaluation of the new capture vapourizer for aerosol mass spectrometers (AMS) through laboratory studies of inorganic species. *Atmos. Meas. Tech.* **2017**, *10*, 2897−2921.
(33) Zhang, Y.; Tang, L.; Croteau, P. L.; Favez, O.; Sun, Y.; Canagaratna, M. R.; Wang, Z.; Couvidat, F.; Albinet, A.; Zhang, H.; Sciare, J.; Prévôt, A. S. H.; Jayne, J. T.; Worsnop, D. R. Field characterization of the PM2.5 Aerosol Chemical Speciation Monitor: insights into the composition, sources, and processes of fine particles in eastern China. *Atmos. Chem. Phys.* **2017**, *17*, 14501−14517.
(34) Xu, W.; Croteau, P.; Williams, L.; Canagaratna, M.; Onasch, T.; Cross, E.; Zhang, X.; Robinson, W.; Worsnop, D.; Jayne, J. Laboratory characterization of an aerosol chemical speciation monitor with PM2.5 measurement capability. *Aerosol Sci. Technol.* **2017**, *51*, 69−83.
(35) Hu, W.; Campuzano-Jost, P.; Day, D. A.; Croteau, P.; Canagaratna, M. R.; Jayne, J. T.; Worsnop, D. R.; Jimenez, J. L. Evaluation of the new capture vaporizer for aerosol mass spectrometers (AMS) through field studies of inorganic species. *Aerosol Sci. Technol.* **2017**, *51*, 735−754.
(36) Hu, W.; Day, D. A.; Campuzano-Jost, P.; Nault, B. A.; Park, T.; Lee, T.; Croteau, P.; Canagaratna, M. R.; Jayne, J. T.; Worsnop, D. R.; Jimenez, J. L. Evaluation of the new capture vaporizer for aerosol mass spectrometers: Characterization of organic aerosol mass spectra. *Aerosol Sci. Technol.* **2018**, *52*, 725−739.
(37) Hu, W.; Day, D. A.; Campuzano-Jost, P.; Nault, B. A.; Park, T.; Lee, T.; Croteau, P.; Canagaratna, M. R.; Jayne, J. T.; Worsnop, D. R.; Jimenez, J. L. Evaluation of the New Capture Vaporizer for Aerosol Mass Spectrometers (AMS): Elemental Composition and Source Apportionment of Organic Aerosols (OA). *ACS Earth Space Chem.* **2018**, *2*, 410−421.
(38) Carlton, A. G.; de Gouw, J.; Jimenez, J. L.; Ambrose, J. L.; Attwood, A. R.; Brown, S.; Baker, K. R.; Brock, C.; Cohen, R. C.; Edgerton, S.; Farkas, C. M.; Farmer, D.; Goldstein, A. H.; Gratz, L.; Guenther, A.; Hunt, S.; Jaeglé, L.; Jaffe, D. A.; Mak, J.; McClure, C.; Nenes, A.; Nguyen, T. K.; Pierce, J. R.; de Sa, S.; Selin, N. E.; Shah, V.; Shaw, S.; Shepson, P. B.; Song, S.; Stutz, J.; Surratt, J. D.; Turpin, B. J.; Warneke, C.; Washenfelder, R. A.; Wennberg, P. O.; Zhou, X. Synthesis of the Southeast Atmosphere Studies: Investigating Fundamental Atmospheric Chemistry Questions. *Bull. Am. Meteorol. Soc.* **2018**, *99*, 547−567.
(39) Hu, W. W.; Campuzano-Jost, P.; Palm, B. B.; Day, D. A.; Ortega, A. M.; Hayes, P. L.; Krechmer, J. E.; Chen, Q.; Kuwata, M.; Liu, Y. J.; de Sá, S. S.; McKinney, K.; Hu, M.; Budisulistiorini, S. H.; Riva, M.; Surratt, J. D.; St. Clair, J. M.; Isaacman-Van Wertz, G.; Yee, L. D.; Goldstein, A. H.; Carbone, S.; Brito, J.; Artaxo, P.; de Gouw, J. A.; Koss, A.; Wisthaler, A.; Mikoviny, T.; Karl, T.; Kaser, L.; Jud, W.; Hansel, A.; Docherty, K. S.; Alexander, M. L.; Robinson, N. H.; Coe, H.; Allan, J. D.; Canagaratna, M. R.; Paulot, F.; Jimenez, J. L.; Jimenez, J. L. Characterization of a real-time tracer for isoprene epoxydiols-derived secondary organic aerosol (IEPOX-SOA) from aerosol mass spectrometer measurements. *Atmos. Chem. Phys.* **2015**, *15*, 11807−11833.
(40) Xu, L.; Guo, H.; Boyd, C. M.; Klein, M.; Bougiatioti, A.; Cerully, K. M.; Hite, J. R.; Isaacman-VanWertz, G.; Kreisberg, N. M.; Knote, C.; Olson, K.; Koss, A.; Goldstein, A. H.; Hering, S. V.; de Gouw, J.; Baumann, K.; Lee, S.-H.; Nenes, A.; Weber, R. J.; Ng, N. L. Effects of anthropogenic emissions on aerosol formation from isoprene and monoterpenes in the southeastern United States. *Proc. Natl. Acad. Sci. U.S.A.* **2014**, *112*, 37−42.
(41) Ayres, B. R.; Allen, H. M.; Draper, D. C.; Brown, S. S.; Wild, R. J.; Jimenez, J. L.; Day, D. A.; Campuzano-Jost, P.; Hu, W.; de Gouw, J.; Koss, A.; Cohen, R. C.; Duffey, K. C.; Romer, P.; Baumann, K.; Edgerton, E.; Takahama, S.; Thornton, J. A.; Lee, B. H.; Lopez-Hilfiker, F. D.; Mohr, C.; Wennberg, P. O.; Nguyen, T. B.; Teng, A.; Goldstein, A. H.; Olson, K.; Fry, J. L. Organic nitrate aerosol formation via NO3 + biogenic volatile organic compounds in the southeastern United States. *Atmos. Chem. Phys.* **2015**, *15*, 13377−13392.
(42) Zhang, H.; Yee, L. D.; Lee, B. H.; Curtis, M. P.; Worton, D. R.; Isaacman-VanWertz, G.; Offenberg, J. H.; Lewandowski, M.; Kleindienst, T. E.; Beaver, M. R.; Holder, A. L.; Lonneman, W. A.; Docherty, K. S.; Jaoui, M.; Pye, H. O. T.; Hu, W.; Day, D. A.; Campuzano-Jost, P.; Jimenez, J. L.; Guo, H.; Weber, R. J.; de Gouw, J.; Koss, A. R.; Edgerton, E. S.; Brune, W.; Mohr, C.; Lopez-Hilfiker, F. D.; Lutz, A.; Kreisberg, N. M.; Spielman, S. R.; Hering, S. V.; Wilson, K. R.; Thornton, J. A.; Goldstein, A. H. Monoterpenes are the largest source of summertime organic aerosol in the southeastern United States. *Proc. Natl. Acad. Sci. U.S.A.* **2018**, *115*, 2038−2043.
(43) Kim, P. S.; Jacob, D. J.; Fisher, J. A.; Travis, K.; Yu, K.; Zhu, L.; Yantosca, R. M.; Sulprizio, M. P.; Jimenez, J. L.; Campuzano-Jost, P.; Froyd, K. D.; Liao, J.; Hair, J. W.; Fenn, M. A.; Butler, C. F.; Wagner,

N. L.; Gordon, T. D.; Welti, A.; Wennberg, P. O.; Crounse, J. D.; St. Clair, J. M.; Teng, A. P.; Millet, D. B.; Schwarz, J. P.; Markovic, M. Z.; Perring, A. E. Sources, seasonality, and trends of southeast US aerosol: an integrated analysis of surface, aircraft, and satellite observations with the GEOS-Chem chemical transport model. *Atmos. Chem. Phys.* **2015**, *15*, 10411−10433.

(44) Mao, J.; Carlton, A.; Cohen, R. C.; Brune, W. H.; Brown, S. S.; Wolfe, G. M.; Jimenez, J. L.; Pye, H. O. T.; Lee Ng, N.; Xu, L.; McNeill, V. F.; Tsigaridis, K.; McDonald, B. C.; Warneke, C.; Guenther, A.; Alvarado, M. J.; de Gouw, J.; Mickley, L. J.; Leibensperger, E. M.; Mathur, R.; Nolte, C. G.; Portmann, R. W.; Unger, N.; Tosca, M.; Horowitz, L. W. Southeast Atmosphere Studies: learning from model-observation syntheses. *Atmos. Chem. Phys.* **2018**, *18*, 2615−2651.

(45) Kim, H.; Zhang, Q.; Heo, J. Influence of Intense secondary aerosol formation and long range transport on aerosol chemistry and properties in the Seoul Metropolitan Area during spring time: Results from KORUS-AQ. *Atmos. Chem. Phys.* **2018**, *18*, 7149.

(46) Nault, B. A.; Campuzano-Jost, P.; Day, D. A.; Schroder, J. C.; Anderson, B.; Beyersdorf, A. J.; Blake, D. R.; Brune, W. H.; Choi, Y.; Corr, C. A.; de Gouw, J. A.; Dibb, J.; DiGangi, J. P.; Diskin, G. S.; Fried, A.; Huey, L. G.; Kim, M. J.; Knote, C. J.; Lamb, K. D.; Lee, T.; Park, T.; Pusede, S. E.; Scheuer, E.; Thornhill, K. L.; Woo, J.-H.; Jimenez, J. L. Secondary Organic Aerosol Production from Local Emissions Dominates the Organic Aerosol Budget over Seoul, South Korea, during KORUS-AQ. *Atmos. Chem. Phys.* **2018**, *18*, 17769−17800.

(47) DeCarlo, P. F.; Kimmel, J. R.; Trimborn, A.; Northway, M. J.; Jayne, J. T.; Aiken, A. C.; Gonin, M.; Fuhrer, K.; Horvath, T.; Docherty, K. S.; Worsnop, D. R.; Jimenez, J. L. Field-deployable, high-resolution, time-of-flight aerosol mass spectrometer. *Anal. Chem.* **2006**, *78*, 8281−8289.

(48) Jimenez, J. L.; Canagaratna, M. R.; Drewnick, F.; Allan, J. D.; Alfarra, M. R.; Middlebrook, A. M.; Slowik, J. G.; Zhang, Q.; Coe, H.; Jayne, J. T.; Worsnop, D. R. Comment on "The effects of molecular weight and thermal decomposition on the sensitivity of a thermal desorption aerosol mass spectrometer". *Aerosol Sci. Technol.* **2016**, *50*, 1−15.

(49) Xu, W.; Lambe, A.; Silva, P.; Hu, W.; Onasch, T.; Williams, L.; Croteau, P.; Zhang, X.; Renbaum-Wolff, L.; Fortner, E.; Jimenez, J. L.; Jayne, J.; Worsnop, D.; Canagaratna, M. Laboratory evaluation of species-dependent relative ionization efficiencies in the Aerodyne Aerosol Mass Spectrometer. *Aerosol Sci. Technol.* **2018**, *52* (6), 626−641.

(50) Xu, W.; Lambe, A.; Silva, P.; Hu, W.; Onasch, T.; Williams, L.; Croteau, P.; Zhang, X.; Renbaum-Wolff, L.; Fortner, E.; Jimenez, J. L.; Jayne, J.; Worsnop, D.; Canagaratna, M. Laboratory evaluation of species-dependent relative ionization efficiencies in the Aerodyne Aerosol Mass Spectrometer. *Aerosol Sci. Technol.* **2018**, *52*, 626−641.

(51) Canagaratna, M. R.; Jimenez, J. L.; Kroll, J. H.; Chen, Q.; Kessler, S. H.; Massoli, P.; Hildebrandt Ruiz, L.; Fortner, E.; Williams, L. R.; Wilson, K. R.; Surratt, J. D.; Donahue, N. M.; Jayne, J. T.; Worsnop, D. R. Elemental ratio measurements of organic compounds using aerosol mass spectrometry: characterization, improved calibration, and implications. *Atmos. Chem. Phys.* **2015**, *15*, 253−272.

(52) Kang, E.; Root, M. J.; Toohey, D. W.; Brune, W. H. Introducing the concept of Potential Aerosol Mass (PAM). *Atmos. Chem. Phys.* **2007**, *7*, 5727−5744.

(53) Lambe, A. T.; Onasch, T. B.; Massoli, P.; Croasdale, D. R.; Wright, J. P.; Ahern, A. T.; Williams, L. R.; Worsnop, D. R.; Brune, W. H.; Davidovits, P. Laboratory studies of the chemical composition and cloud condensation nuclei (CCN) activity of secondary organic aerosol (SOA) and oxidized primary organic aerosol (OPOA). *Atmos. Chem. Phys.* **2011**, *11*, 8913−8928.

(54) Li, R.; Palm, B. B.; Ortega, A. M.; Hlywiak, J.; Hu, W.; Peng, Z.; Day, D. A.; Knote, C.; Brune, W. H.; de Gouw, J. A.; Jimenez, J. L. Modeling the Radical Chemistry in an Oxidation Flow Reactor: Radical Formation and Recycling, Sensitivities, and OH Exposure Estimation Equation. *J. Phys. Chem. A* **2015**, *119*, 4418−4432.

(55) Palm, B. B.; Campuzano-Jost, P.; Ortega, A. M.; Day, D. A.; Kaser, L.; Jud, W.; Karl, T.; Hansel, A.; Hunter, J. F.; Cross, E. S.; Kroll, J. H.; Peng, Z.; Brune, W. H.; Jimenez, J. L. In situ secondary organic aerosol formation from ambient pine forest air using an oxidation flow reactor. *Atmos. Chem. Phys.* **2016**, *16*, 2943−2970.

(56) Palm, B. B.; de Sá, S. S.; Campuzano-Jost, P.; Hu, W.; Seco, R.; Sjostedt, S. J.; Park, J.-H.; Guenther, A. B.; Kim, S.; Brito, J.; Wurm, F.; Artaxo, P.; Thalman, R.; Wang, J.; Yee, L. D.; Wernis, R.; Isaacman-VanWertz, G.; Goldstein, A. H.; Liu, Y.; Springston, S. R.; Souza, R.; Newburn, M. K.; Alexander, M. L.; Martin, S. T.; Jimenez, J. L.; Jimenez, J. L. Secondary organic aerosol formation from ambient air in an oxidation flow reactor in central Amazonia. *Atmos. Chem. Phys.* **2018**, *18*, 467−493.

(57) Hu, W.; Palm, B. B.; Day, D. A.; Campuzano-Jost, P.; Krechmer, J. E.; Peng, Z.; de Sá, S. S.; Martin, S. T.; Baumann, K.; Hacker, L.; Kiendler-Scharr, A.; Koss, A. R.; de Gouw, J. A.; Goldstein, A. H.; Seco, R.; Sjostedt, S. J.; Park, J.-H.; Guenther, A. B.; Kim, S.; Canonaco, F.; Prévôt, A. S. H.; Brune, W. H.; Jimenez, J. L.; Jimenez, J. L. Volatility and lifetime against OH heterogeneous reaction of ambient isoprene-epoxydiols-derived secondary organic aerosol (IEPOX-SOA). *Atmos. Chem. Phys.* **2016**, *16*, 11563−11580.

(58) Ortega, A. M.; Hayes, P. L.; Peng, Z.; Palm, B. B.; Hu, W.; Day, D. A.; Li, R.; Cubison, M. J.; Brune, W. H.; Graus, M.; Warneke, C.; Gilman, J. B.; Kuster, W. C.; de Gouw, J.; Gutiérrez-Montes, C.; Jimenez, J. L. Real-time measurements of secondary organic aerosol formation and aging from ambient air in an oxidation flow reactor in the Los Angeles area. *Atmos. Chem. Phys.* **2016**, *16*, 7411−7433.

(59) Huffman, J. A.; Ziemann, P. J.; Jayne, J. T.; Worsnop, D. R.; Jimenez, J. L. Development and Characterization of a Fast-Stepping/Scanning Thermodenuder for Chemically-Resolved Aerosol Volatility Measurements. *Aerosol Sci. Technol.* **2008**, *42*, 395.

(60) Peng, Z.; Day, D. A.; Stark, H.; Li, R.; Lee-Taylor, J.; Palm, B. B.; Brune, W. H.; Jimenez, J. L. HOx radical chemistry in oxidation flow reactors with low-pressure mercury lamps systematically examined by modeling. *Atmos. Meas. Tech.* **2015**, *8*, 4863−4890.

(61) Palm, B. B.; Campuzano-Jost, P.; Day, D. A.; Ortega, A. M.; Fry, J. L.; Brown, S. S.; Zarzana, K. J.; Dube, W.; Wagner, N. L.; Draper, D. C.; Kaser, L.; Jud, W.; Karl, T.; Hansel, A.; Gutiérrez-Montes, C.; Jimenez, J. L. Secondary organic aerosol formation from in situ OH, O3, and NO3 oxidation of ambient forest air in an oxidation flow reactor. *Atmos. Chem. Phys.* **2017**, *17*, 5331−5354.

(62) Cappa, C. D.; Jimenez, J. L. Quantitative estimates of the volatility of ambient organic aerosol. *Atmos. Chem. Phys.* **2010**, *10*, 5409−5424.

(63) Faulhaber, A. E.; Thomas, B. M.; Jimenez, J. L.; Jayne, J. T.; Worsnop, D. R.; Ziemann, P. J. Characterization of a thermodenuder-particle beam mass spectrometer system for the study of organic aerosol volatility and composition. *Atmos. Meas. Tech.* **2009**, *2*, 15−31.

(64) Huffman, J. A.; Docherty, K. S.; Aiken, A. C.; Cubison, M. J.; Ulbrich, I. M.; DeCarlo, P. F.; Sueper, D.; Jayne, J. T.; Worsnop, D. R.; Ziemann, P. J.; Jimenez, J. L. Chemically-resolved aerosol volatility measurements from two megacity field studies. *Atmos. Chem. Phys.* **2009**, *9*, 7161−7182.

(65) DeCarlo, P. F.; Dunlea, E. J.; Kimmel, J. R.; Aiken, A. C.; Sueper, D.; Crounse, J.; Wennberg, P. O.; Emmons, L.; Shinozuka, Y.; Clarke, A.; Zhou, J.; Tomlinson, J.; Collins, D. R.; Knapp, D.; Weinheimer, A. J.; Montzka, D. D.; Campos, T.; Jimenez, J. L. Fast airborne aerosol size and chemistry measurements above Mexico City and Central Mexico during the MILAGRO campaign. *Atmos. Chem. Phys.* **2008**, *8*, 4027−4048.

(66) Salcedo, D.; Onasch, T. B.; Dzepina, K.; Canagaratna, M. R.; Zhang, Q.; Huffman, J. A.; DeCarlo, P. F.; Jayne, J. T.; Mortimer, P.; Worsnop, D. R.; Kolb, C. E.; Johnson, K. S.; Zuberi, B.; Marr, L. C.; Volkamer, R.; Molina, L. T.; Molina, M. J.; Cardenas, B.; Bernabé, R. M.; Márquez, C.; Gaffney, J. S.; Marley, N. A.; Laskin, A.; Shutthanandan, V.; Xie, Y.; Brune, W.; Lesher, R.; Shirley, T.; Jimenez, J. L. Characterization of ambient aerosols in Mexico City during the MCMA-2003 campaign with Aerosol Mass Spectrometry:

https://dx.doi.org/10.1021/acsearthspacechem.9b00310
ACS Earth Space Chem. 2020, 4, 676−689

results from the CENICA Supersite. *Atmos. Chem. Phys.* **2006**, *6*, 925−946.
(67) DeCarlo, P. F.; Slowik, J. G.; Worsnop, D. R.; Davidovits, P.; Jimenez, J. L. Particle morphology and density characterization by combined mobility and aerodynamic diameter measurements. Part 1: Theory. *Aerosol Sci. Technol.* **2004**, *38*, 1185−1205.
(68) Sullivan, A. P.; Weber, R. J.; Clements, A. L.; Turner, J. R.; Bae, M. S.; Schauer, J. J. A method for on-line measurement of water-soluble organic carbon in ambient aerosol particles: Results from an urban site. *Geophys. Res. Lett.* **2004**, *31*, L13105.
(69) Xu, L.; Guo, H.; Weber, R. J.; Ng, N. L. Chemical Characterization of Water-Soluble Organic Aerosol in Contrasting Rural and Urban Environments in the Southeastern United States. *Environ. Sci. Technol.* **2017**, *51*, 78−88.
(70) Murphy, D. M. The effects of molecular weight and thermal decomposition on the sensitivity of a thermal desorption aerosol mass spectrometer. *Aerosol Sci. Technol.* **2016**, *50*, 118−125.
(71) Murphy, D. M. Reply to "Comment on the effects of molecular weight and thermal decomposition on the sensitivity of a thermal desorption aerosol mass spectrometer" by Jimenez et al. *Aerosol Sci. Technol.* **2016**, *50*, 1277.
(72) Reyes-Villegas, E.; Bannan, T.; Le Breton, M.; Mehra, A.; Priestley, M.; Percival, C.; Coe, H.; Allan, J. D. Online Chemical Characterization of Food-Cooking Organic Aerosols: Implications for Source Apportionment. *Environ. Sci. Technol.* **2018**, *52*, 5308−5318.
(73) Huffman, J. A.; Jayne, J. T.; Drewnick, F.; Aiken, A. C.; Onasch, T.; Worsnop, D. R.; Jimenez, J. L. Design, modeling, optimization, and experimental tests of a particle beam width probe for the aerodyne aerosol mass spectrometer. *Aerosol Sci. Technol.* **2005**, *39*, 1143−1163.
(74) Takegawa, N.; Miyazaki, Y.; Kondo, Y.; Komazaki, Y.; Miyakawa, T.; Jimenez, J. L.; Jayne, J. T.; Worsnop, D. R.; Allan, J. D.; Weber, R. J. Characterization of an Aerodyne Aerosol Mass Spectrometer (AMS): Intercomparison with other aerosol instruments. *Aerosol Sci. Technol.* **2005**, *39*, 760−770.
(75) Timonen, H.; Aurela, M.; Carbone, S.; Saarnio, K.; Saarikoski, S.; Mäkelä, T.; Kulmala, M.; Kerminen, V.-M.; Worsnop, D. R.; Hillamo, R. High time-resolution chemical characterization of the water-soluble fraction of ambient aerosols with PILS-TOC-IC and AMS. *Atmos. Meas. Tech.* **2010**, *3*, 1063−1074.
(76) Setyan, A.; Zhang, Q.; Merkel, M.; Knighton, W. B.; Sun, Y.; Song, C.; Shilling, J. E.; Onasch, T. B.; Herndon, S. C.; Worsnop, D. R.; Fast, J. D.; Zaveri, R. A.; Berg, L. K.; Wiedensohler, A.; Flowers, B. A.; Dubey, M. K.; Subramanian, R. Characterization of submicron particles influenced by mixed biogenic and anthropogenic emissions using high-resolution aerosol mass spectrometry: results from CARES. *Atmos. Chem. Phys.* **2012**, *12*, 8131−8156.
(77) Liu, P. S. K.; Deng, R.; Smith, K. A.; Williams, L. R.; Jayne, J. T.; Canagaratna, M. R.; Moore, K.; Onasch, T. B.; Worsnop, D. R.; Deshler, T. Transmission efficiency of an aerodynamic focusing lens system: Comparison of model calculations and laboratory measurements for the Aerodyne Aerosol Mass Spectrometer. *Aerosol Sci. Technol.* **2007**, *41*, 721−733.
(78) Salcedo, D.; Onasch, T. B.; Canagaratna, M. R.; Dzepina, K.; Huffman, J. A.; Jayne, J. T.; Worsnop, D. R.; Kolb, C. E.; Weimer, S.; Drewnick, F.; Allan, J. D.; Delia, A. E.; Jimenez, J. L. Technical Note: Use of a beam width probe in an Aerosol Mass Spectrometer to monitor particle collection efficiency in the field. *Atmos. Chem. Phys.* **2007**, *7*, 549−556.
(79) Knote, C.; Brunner, D.; Vogel, H.; Allan, J.; Asmi, A.; Äijälä, M.; Carbone, S.; van der Gon, H. D.; Jimenez, J. L.; Kiendler-Scharr, A.; Mohr, C.; Poulain, L.; Prévôt, A. S. H.; Swietlicki, E.; Vogel, B. Towards an online-coupled chemistry-climate model: evaluation of trace gases and aerosols in COSMO-ART. *Geosci. Model Dev.* **2011**, *4*, 1077−1102.
(80) Ide, Y.; Uchida, K.; Takegawa, N. Ionization efficiency of evolved gas molecules from aerosol particles in a thermal desorption aerosol mass spectrometer: Numerical simulations. *Aerosol Sci. Technol.* **2019**, *53*, 843−852.
(81) Uchida, K.; Ide, Y.; Takegawa, N. Ionization efficiency of evolved gas molecules from aerosol particles in a thermal desorption aerosol mass spectrometer: Laboratory experiments. *Aerosol Sci. Technol.* **2019**, *53*, 86−93.
(82) Pajunoja, A.; Hu, W.; Leong, Y. J.; Taylor, N. F.; Miettinen, P.; Palm, B. B.; Mikkonen, S.; Collins, D. R.; Jimenez, J. L.; Virtanen, A. Phase state of ambient aerosol linked with water uptake and chemical aging in the southeastern US. *Atmos. Chem. Phys.* **2016**, *16*, 11163−11176.
(83) Virtanen, A.; Joutsensaari, J.; Koop, T.; Kannosto, J.; Yli-Pirilä, P.; Leskinen, J.; Mäkelä, J. M.; Holopainen, J. K.; Pöschl, U.; Kulmala, M.; Worsnop, D. R.; Laaksonen, A. An amorphous solid state of biogenic secondary organic aerosol particles. *Nature* **2010**, *467*, 824−827.
(84) Saukko, E.; Lambe, A. T.; Massoli, P.; Koop, T.; Wright, J. P.; Croasdale, D. R.; Pedernera, D. A.; Onasch, T. B.; Laaksonen, A.; Davidovits, P.; Worsnop, D. R.; Virtanen, A. Humidity-dependent phase state of SOA particles from biogenic and anthropogenic precursors. *Atmos. Chem. Phys.* **2012**, *12*, 7517−7529.
(85) You, Y.; Smith, M. L.; Song, M.; Martin, S. T.; Bertram, A. K. Liquid−liquid phase separation in atmospherically relevant particles consisting of organic species and inorganic salts. *Int. Rev. Phys. Chem.* **2014**, *33*, 43−77.
(86) Kolesar, K. R.; Li, Z.; Wilson, K. R.; Cappa, C. D. Heating-Induced Evaporation of Nine Different Secondary Organic Aerosol Types. *Environ. Sci. Technol.* **2015**, *49*, 12242−12252.
(87) Cappa, C. D.; Wilson, K. R. Evolution of organic aerosol mass spectra upon heating: implications for OA phase and partitioning behavior. *Atmos. Chem. Phys.* **2011**, *11*, 1895−1911.
(88) Yli-Juuti, T.; Pajunoja, A.; Tikkanen, O.-P.; Buchholz, A.; Faiola, C.; Väisänen, O.; Hao, L.; Kari, E.; Peräkylä, O.; Garmash, O.; Shiraiwa, M.; Ehn, M.; Lehtinen, K.; Virtanen, A. Factors controlling the evaporation of secondary organic aerosol from α-pinene ozonolysis. *Geophys. Res. Lett.* **2017**, *44*, 2562−2570.
(89) Washenfelder, R. A.; Attwood, A. R.; Brock, C. A.; Guo, H.; Xu, L.; Weber, R. J.; Ng, N. L.; Allen, H. M.; Ayres, B. R.; Baumann, K.; Cohen, R. C.; Draper, D. C.; Duffey, K. C.; Edgerton, E.; Fry, J. L.; Hu, W. W.; Jimenez, J. L.; Palm, B. B.; Romer, P.; Stone, E. A.; Wooldridge, P. J.; Brown, S. S. Biomass burning dominates brown carbon absorption in the rural southeastern United States. *Geophys. Res. Lett.* **2015**, *42*, 653−664.

https://dx.doi.org/10.1021/acsearthspacechem.9b00310
ACS Earth Space Chem. 2020, 4, 676−689